Reprinted from Applied Optics, Vol. 23, page 1206, April 15, 1984

Optical constants of ice from the ultraviolet to the microwave

Stephen G. Warren

A compilation of the optical constants of ice Ih is made for temperatures within 60 K of the melting point. The imaginary part m_{im} of the complex index of refraction m is obtained from measurements of spectral absorption coefficient; the real part m_{re} is computed to be consistent with m_{im} by use of known dispersion relations. The compilation of m_{im} requires subjective interpolation in the near-ultraviolet and microwave, a temperature correction in the far-infrared, and a choice between two conflicting sources in the near-infrared. New measurements of the spectral absorption coefficient of pure ice are needed, at temperatures near the melting point, for 185–400-nm, 1.4–2.8-μm, 3.5–4.3-μm, 33–600-μm, and 1–100-mm wavelengths.

I. Introduction

Theoretical calculations of absorption, transmission, reflection, emission, and scattering of electromagnetic radiation in ice, and in ice-containing media such as snow and clouds, require knowledge of the laboratory measurements of the complex refractive index m of pure ice as a function of wavelength. m is a complex function, $m(\lambda) = m_{re}(\lambda) - im_{im}(\lambda)$, where λ is the wavelength in vacuum, m_{re} is the usual refractive index which determines the phase speed, and m_{im} is related to the absorption coefficient k_{abs}, as $k_{\text{abs}} = 4\pi m_{im}/\lambda$. (We will often refer to the imaginary part of the complex index of refraction as the imaginary index of refraction, and similarly for the real part.) In the microwave and radiowave spectra it is more usual to report the complex relative permittivity $\varepsilon = \varepsilon' - i\varepsilon''$, or the dielectric constant ε' and loss tangent, $\tan\delta \equiv \varepsilon''/\varepsilon'$. In nonmagnetic materials (such as ice) they are related to the complex refractive index m which we report as $m^2 = \varepsilon$.

A. Earlier Reviews

The optical constants of ice have been reviewed by Irvine and Pollack[1] (IP) for the infrared, by Evans[2] for the microwave and radiowave regions, and by Ray[3] and by Hobbs[4] for the entire spectrum. The data recommended by IP have been superseded by better measurements everywhere except in the 1.4–2.8-μm region. Ray fitted analytical formulas to the compilation of IP and to a few points in the microwave, but he ignored Evans's earlier review of the other available microwave data. Hobbs's review is essentially complete up to 1972. In 1980, Wiscombe and Warren[5] compiled the optical constants for the visible and near-infrared, but that compilation also has been superseded by new measurements. There are now many new measurements available with which to prepare a better compilation of m from the far-ultraviolet through the far-infrared. However, there has been little additional reliable work on microwave optical properties of ice since Evans's (1965) review, so for that part of the spectrum we rely mostly on the references which he cited.

B. Crystal Forms of Ice

About ten different phases of ice have been discovered, but most of them can occur only at very high pressure and have only been observed in the laboratory. The three which exist at low pressures are ordinary hexagonal ice Ih; the cubic form ice Ic which can remain stable at temperatures as high as −80°C but must be formed by condensation of vapor at lower temperatures; and amorphous (or vitreous) ice, which forms by condensation of vapor at even lower temperatures. The only form ever observed to occur naturally on earth is ice Ih. Temperatures in tropical cirrus clouds may be cold enough to contain ice Ic, and Whalley[6] has speculated that ice Ic could be responsible for a rare halo that cannot be explained by hexagonal crystals. However, even if that speculation is correct, it does not complicate our specification of the optical constants: in the spectral regions where optical properties of both Ih and Ic have been measured (ultraviolet and far-infrared, as discussed below) they are practically identical. The high-pressure forms of ice also do not exist naturally on earth. Even under the deepest parts of the Antarctic ice sheet, the pressures are insufficient to form ice II or ice III. This review is therefore restricted to the optical

The author is with University of Washington, Department of Atmospheric Sciences, Seattle, Washington 98195.
Received 28 October 1983.
0003-6935/84/081206-20$02.00/0.

properties of ice Ih, but the results can probably be used for Ic as well.

The ice crystal is very slightly birefringent, so that the refractive index varies with orientation of the crystal and polarization of the light. However, the birefringence is so slight that we may safely ignore it. This has been shown by measurements of m on single crystals both in the ultraviolet[7] and in the far-infrared.[8] Thus we are able to use measurements made either on single crystals or on polycrystalline ice (bulk ice made up of crystals whose axes do not coincide), and we need not report two different sets of optical constants. [The reasons for near-isotropy of the ice crystal to radiation are explained by Johari[9] (p. 631).]

C. Features of the Ice Spectrum

The causes of the variation of m with wavelength for ice have been reviewed by Johari.[9] Ice exhibits strong absorption in the ultraviolet (UV) at $\lambda < 170$ nm, due to electronic transitions. Ice is very transparent in the visible, m_{im} reaching its minimum value at $\lambda = 460$ nm. There are weak absorption bands in the near-infrared at $\lambda > 1.4$ μm, which have not been assigned to particular vibrational transitions. The very strong band at $\lambda \simeq 3$ μm is due to vibrational modes involving stretching of the O–H covalent bond. A band at 12 μm is due to rotational oscillation (libration). Up to this wavelength the spectrum of ice shows similarities to the spectra of liquid water and water vapor. The strong far-infrared absorption bands at 45 and 60 μm, however, are due to lattice vibrations which have no counterpart in water vapor, and the spectrum of liquid water is also quite different in this region. The absorptivity again drops to low values in the microwave region, and remains small until the dielectric relaxation peak is approached at a frequency of ~3 kHz (wavelength 100 km). The dielectric relaxation of liquid water, by contrast, occurs at $\lambda \simeq 20$ mm.[3] The dielectric properties of ice and water are therefore dramatically different over ~7 orders of magnitude in frequency in the microwave and radiowave regions; water is highly reflective, but ice is quite transparent.

D. Measurements: Purposes and Methods

This review is written with geophysical applications in mind, so emphasis is placed on obtaining the optical constants for temperatures T between 0° and −60°C. In this high-temperature region, the temperature dependence of the optical constants is poorly known. However, based on suggestive evidence from near-ultraviolet and far-infrared measurements discussed below, the temperature dependence for $\lambda < 100$ μm is likely to be small within 60 K of the melting point. At longer wavelengths, m_{im} becomes increasingly sensitive to temperature as λ increases. We report a temperature-dependent m for $\lambda > 167$ μm, tabulating it at four temperatures: −1°, −5°, −20°, −60°C. For $\lambda < 167$ μm we attempt a compilation only for one temperature, $T = -7$°C, which is the temperature of Schaaf and Williams's[10] infrared measurements, but we expect it to be valid for most temperatures that would be found on earth.

Unfortunately for geophysical applications, much of the spectrum of ice has been measured only at temperatures much colder than any terrestrial temperatures, and we must attempt to adjust these results to values appropriate for warmer temperatures. Many of the measurements we use were made not for the purpose of geophysical application, but rather to understand the behavior of the water molecule within the ice lattice. The spectra are usually easier to interpret at lower temperatures. Studies of the electronic structure in the ultraviolet[7] were thus made at 80 K; studies of the lattice vibrations in the far-infrared[11] were made at 100 K. Measurements at temperatures near 0°C were made in the visible, near-infrared, middle-infrared, and radiowave regions. No reliable measurements of m are available at any temperature for the near-ultraviolet between 185 and 400 μm and in the microwave between 1.25 and 32 mm. In these regions we must obtain the absorption coefficient by a subjective interpolation.

In spectral regions where $m_{im} \ll m_{re}$, m_{im} is determined by attenuation of a beam of light through a block of clear bubble-free ice. Blocks as long as 2.8 m were needed by Grenfell and Perovich[12] to obtain sufficient attenuation for accurate measurement in the visible wavelengths where ice is very transparent. Films as thin as 50 μm are needed to obtain sufficient transmission at 1–2-μm wavelength. In the far-infrared, Bertie *et al.*[11] used some ice films that were <1 μm in thickness. In the latter cases the uncertainty in measurement of sample thickness limits the accuracy of m_{im}.

The real index m_{re} is obtained by reflectance measurements from a plane-shave ice block. The Fresnel formulas give m_{re} unambiguously if m_{im} is small. The real index m_{re} is thus known reliably, and independently of m_{im}, in the regions of weak absorption (visible and microwave).

In regions of large imaginary part ($m_{im} \gtrsim 0.01\, m_{re}$), the Fresnel reflectivity is no longer dominated by m_{re} but also contains a measurable contribution due to m_{im}. A relationship between m_{re} and m_{im} can be obtained by using dispersion analysis.[13] Reflectance measurements can thus be used to determine both m_{re} and m_{im}, but for this method some prior information is also needed about m_{re} or m_{im} outside the region studied.

The real index is of the order unity at all wavelengths short of the dielectric relaxation; the imaginary index, by contrast, varies over the range from 10^{-9} to 10^{0}. The real and imaginary indices are related by the Kramers-Kronig equation:

$$m_{re}(\lambda_0) = 1 + \frac{2\lambda_0^2}{\pi} P \int_0^\infty \frac{m_{im}(\lambda) d\lambda}{\lambda(\lambda_0^2 - \lambda^2)}, \qquad (1)$$

where P indicates the Cauchy principal value of the integral. To compute m_{re} at a particular wavelength, one needs m_{im} at all wavelengths. An analogous equation computes m_{im} by an integral over m_{re}. However, m_{im} cannot be obtained accurately by this method in spectral regions where it is many orders of

magnitude smaller than m_{re}, because m_{re} is known accurately to at most 4 decimal places. By contrast, m_{re} can be obtained reliably from Eq. (1).

E. Compilation Procedure

We follow the approach that Hale and Querry[14] used in their compilation of m for liquid water. We review measurements of m_{im}, displaying them in figures in the regions of disagreement. We compile our best estimate of $m_{im}(\lambda)$ over the entire spectrum of interest. We then compute $m_{re}(\lambda)$ from Eq. (1), making an assumption about the behavior of m_{im} at wavelengths shorter than those measured ($\lambda < 45$ nm) in order to obtain the correct value of m_{re} where it is known in the visible spectrum. Before using Eq. (1) to obtain $m_{re}(\lambda)$, however, it is necessary to correct the far-infrared measurements of $m_{im}(\lambda)$ from 100 K to 266 K. This correction is constrained as follows.

The real index is known independently of m_{im} in regions where $m_{im} \ll m_{re}$. It is ~1.31 in the visible[15] and 1.78 in the microwave.[16] The difference of 0.47 between these values can be attributed to an integral of m_{im} between these two wavelengths, in another Kramers-Kronig relation,

$$m_{re}(\nu_1) - m_{re}(\nu_2) = \frac{1}{2\pi^2} \int_{\nu_1}^{\nu_2} \frac{k_{abs}(\nu)}{\nu^2}\, d\nu, \qquad (2)$$

where $\nu = 1/\lambda$. Since these two values of m_{re} are accurately known, we use them to constrain our correction in the far-infrared from measurements of m_{im} at 100 K to our estimate for 266 K. As explained below, the dominant contributions to the integral in Eq. (2) come from the 40–100-μm region. Our first estimate of the temperature correction gives $k_{abs}(\nu)$ which is slightly inconsistent with Eq. (2); we then adjust the far-infrared spectrum until Eq. (2) is satisfied, before computing $m_{re}(\lambda)$ from Eq. (1).

We start our compilation of m at $\lambda = 45$ nm because there are no quantitative measurements at shorter wavelengths. We terminate it at $\lambda = 8.6$ m. The dielectric properties at longer radio wavelengths have been adequately reviewed by others, including Johari,[9] Evans,[2] Jiracek,[17] and Hasted.[18]

II. Ultraviolet, 44–185 nm

A. Sources of Data

The following references are listed more or less in order of increasing wavelength:

Seki *et al.*[7] (1981) grew a single crystal of hexagonal ice and cooled it to $T = 80$ K for measurement of the reflectivity from 44 to 207 nm, using polarized synchrotron radiation as the light source. Kramers-Kronig analysis was used to obtain ε' and ε''. Usable values of ε'' were obtained only for 44–160 nm, because ε'' becomes too small beyond 160 nm to be constrained by the Kramers-Kronig analysis. The corresponding values of m_{im} are plotted here in Fig. 1. The spectrum was measured for light polarized parallel and perpendicular to the c axis of the crystal, with identical results to within the experimental error of 3%. Amorphous ice was also studied. Its spectrum was somewhat smoother; the peaks at 70 and 140 nm were both weaker.

Daniels[19] (1971) reported energy-loss measurements from fast electrons for ice (probably amorphous) condensed from vapor at $T = 78$ K, obtaining significant absorption values for 8–28 eV (150–44 nm), with 0.4-eV spectral resolution. He obtained the ε' and ε'' by Kramers-Kronig analysis. The corresponding m_{im} is plotted here in Fig. 1.

Onaka and Takahashi[20] (1968) condensed ice at temperatures between 83 and 203 K and measured the UV absorption spectrum from 7 to 10 eV (177–124-nm wavelength). The peak at 144 nm (shown in Fig. 1 here as obtained by other investigators) was found only for temperatures in the range where cubic ice would be expected. However, Daniels[19] found this peak for amorphous ice, and Seki *et al.*[7] found it for both amorphous and hexagonal ice. This discrepancy has not been explained.

Otto and Lynch[21] (1970) measured the electron energy-loss spectrum in the UV (5–35 eV) for ice frozen from liquid water and cooled to −10°C. It was thus probably polycrystalline hexagonal ice. These measurements were unfortunately only qualitative, but they differ notably from those made at lower temperatures: Otto and Lynch found only a shoulder at 144 nm instead of a peak. Daniels[19] speculated that Otto and Lynch's failure to obtain the peak was due to poor spectral resolution, but we cannot rule out the possibility that the spectrum depends on temperature near the melting point.

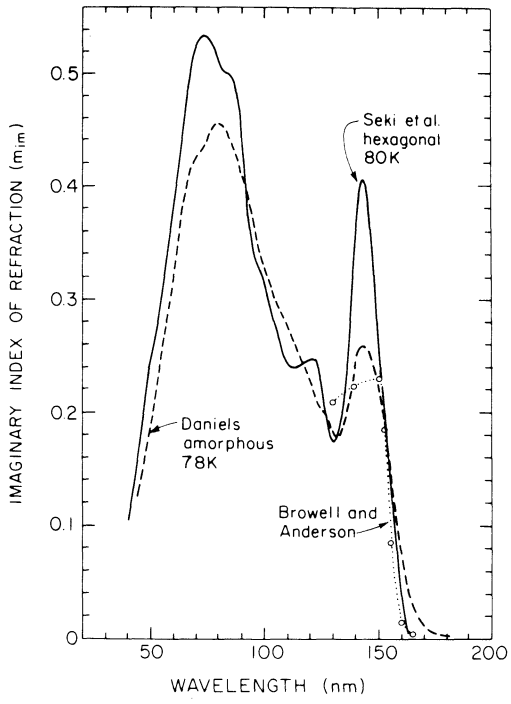

Fig. 1. Imaginary refractive index of ice in the ultraviolet. The measurements of Seki *et al.*[7] are the ones used in our compilation. They are for a hexagonal single crystal at 80 K, both polarizations.

Dressler and Schnepp[22] (1960) deposited ice from the vapor phase at temperatures of 175 K and 77 K and assumed the ice forms to be hexagonal and amorphous, respectively. Transmission measurements were made to obtain the absorption coefficient from 140 to 170 nm. Scattering of light by cracks or bubbles (which would reduce the transmission and lead to an excessive estimate of absorption coefficient) was shown to be negligible by measurements outside the absorption band at longer wavelength. The film thickness was estimated by measuring the amount of vapor deposited. Uncertainty in this quantity leads to an uncertainty in absorption coefficient. The absorption coefficient for amorphous ice at 77 K was found identical to that for hexagonal ice at 175 K over the entire spectral range studied.

Browell and Anderson[23] (1975) grew ice by deposition from the vapor phase. They measured the reflectance at two angles as functions of ice thickness. The period of the interference fringes was used to obtain m_{re} for 161–320-nm wavelength at deposition temperatures 77 K (amorphous) and 155 K (hexagonal). They also obtained an upper limit for the absorption coefficient at one wavelength only (147.5 nm) which they used to correct Dressler and Schnepp's[22] values at all wavelengths 130–170 nm, as shown in Figs. 1 and 2.

Shibaguchi *et al.*[24] (1977, their Fig. 6) measured the absorption spectrum of hexagonal H_2O-ice for 173–178-nm wavelength. (They also measured the 120–160-nm region, but only for D_2O-ice.) The absorption coefficient varies by a factor of ~20 over this wavelength region. The corresponding m_{im} is plotted in Fig. 2 for the two extreme temperatures they used.

Minton[25] (1971) measured the molar extinction coefficient for samples of polycrystalline hexagonal ice 1–10 mm thick at 181–185-nm wavelength. The absorption coefficient varies by a factor of ~20 over this wavelength interval. The samples were frozen from liquid water, then polished; clear samples of measured thickness were chosen. Because of the possibility of some slight scattering of light by the ice, Minton regarded his values as upper limits. The molar extinction coefficient was independent of temperature over the range from −10 to −40°C; the corresponding m_{im} is plotted in Fig. 2.

Painter *et al.*[26] (1969) reviewed measurements of m_{im} for liquid water in the near-UV (their Fig. 9). Measurements from a variety of authors were in substantial agreement. We have drawn a single smooth curve through their Fig. 9 from 160 to 200 nm and included it in our Fig. 2 here, because we will use it in our argument for the interpolation of the ice m_{im}.

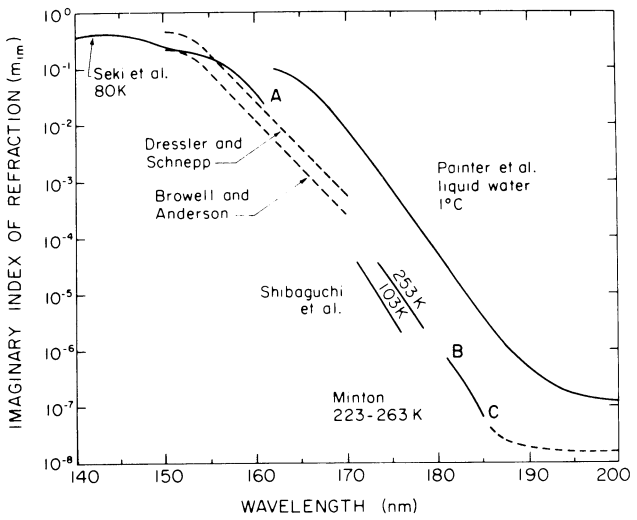

Fig. 2. Imaginary refractive index of ice and water in the ultraviolet. Our compilation uses Seki *et al.*[7] to point *A*, and Minton[25] from point *B* to point *C*, joining point *A* to point *B* by a straight line. The straight line coincides with the 253 K values of Shibaguchi *et al.*[24] The dashed line extending from point *C* to longer wavelengths is our chosen interpolation where no data are available.

B. Compilation of Imaginary Index

The only available measurements of light absorption by hexagonal ice in the ultraviolet short of 130 nm are those of Seki *et al.*[7] They are plotted together with Daniels's[19] measurements in Fig. 1. The values of Seki *et al.* are preferred to those of Daniels because Daniels's spectral resolution was poorer, his measurements used electrons instead of photons, and his ice was probably amorphous rather than hexagonal.

Seki *et al.*'s measurements were taken at 80 K. The spectrum may be somewhat different at higher temperature, but probably not by much, based on the small temperature dependence from 83 to 160 K of the UV spectra of D_2O-ice shown in Fig. 4 of Shibaguchi *et al.*[24] Dressler and Schnepp[22] also found no difference between amorphous ice (77 K) and hexagonal ice (160 K) in their absorption at 140–170 nm. However, all this evidence for weak temperature dependence comes from measurements well below the melting point. The qualitative spectrum of Otto and Lynch[21] near the melting point shows a shoulder instead of a peak at 144 nm. There is thus a need for ultraviolet measurements near the melting point to resolve this discrepancy.

Based on the above discussion, we choose the values of Seki *et al.*[7] for 45–161 nm. Beyond 161 nm, the absorption is too small for m_{im} to be obtained accurately by their reflection measurements. There are short gaps between available measurements (Fig. 2) in the 161–181-nm region. We choose to join points *A* and *B* in Fig. 2 by a straight line. This amounts to assuming that $\ln m_{im}$ varies linearly with wavelength. The parallel behavior of m_{im} of liquid water (also plotted in Fig. 2) serves to justify this. The straight line connects Minton's[25] measurements near the melting point (point *B*) with Seki *et al.*'s measurements at 80 K (point *A*) and passes directly through measurements of Shibaguchi *et al.*[24] close to the melting point. In making this interpolation we choose to ignore Dressler and Schnepp's[22] (DS) data. Browell and Anderson[23] (BA) called them into question as being probably too high and tried to adjust them downward by a dubious *ad hoc* procedure, based on their own estimated upper limit for m_{im} at 147 nm. We choose to ignore the measurements of both DS

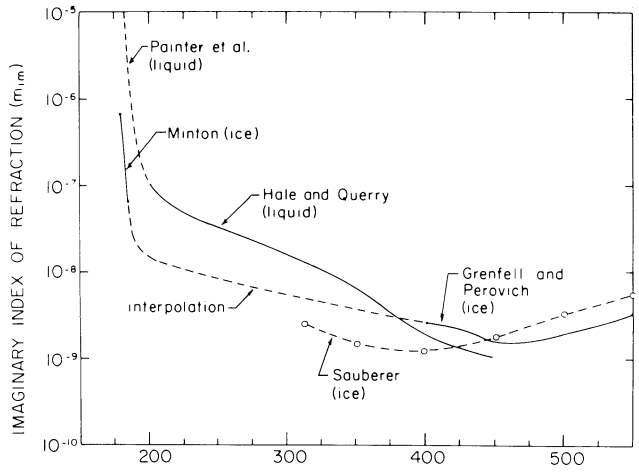

Fig. 3. Imaginary refractive index of ice and water in the near-ultraviolet. Our compilation uses the dashed line to interpolate between Minton[25] at 185-nm and Grenfell and Perovich[12] at 400-nm wavelength.

and BA, but we note that our interpolation passes close to both of their results for 160–170 nm.

III. Visible and Near-Visible, 185–1400 nm

A. Sources of Data

Hale and Querry[14] (1973) reviewed the optical constants of liquid water at 25°C from 200-nm to 200-μm wavelength. In Fig. 3 we have plotted their chosen values for 200–400 nm because we will use them as a guide for interpolation in this spectral region where measurements on ice are lacking.

Sauberer[27] (1950) measured absorption of light through blocks of lake ice 140–500 mm long, for 313–1100-nm wavelength. Although these blocks were apparently very clean and bubble-free, they were not long enough to attenuate the beam by more than 2% in the region of minimum absorption in the visible.

Grenfell and Perovich[12] (1981) measured absorption of light through polycrystalline hexagonal ice at −4°C. To cover the variation of m_{im} over the 400–1400-nm spectral range, three samples of different thickness were used: 2.8 m for 400–850-nm, 200 mm for 700–1100-nm, and 8.2 mm for 1000–1400-nm wavelength. The ice was demonstrated to be almost completely free of bubbles. These measurements supersede those of Sauberer.[27] The wavelength resolution is given by Grenfell[28]: the full bandwidth at half-maximum is ~20 nm at λ = 400 nm and 30 nm at λ = 1400 nm.

B. Compilation of Imaginary Index

There is a gap in measurements between 185 nm (Minton[25]) and 313 nm (Sauberer[27]) where it is difficult to guess the actual behavior of m_{im}. In fact, we choose not to use Sauberer's measurements at all because they disagree by a factor of 2 with the more accurate measurements of Grenfell and Perovich[12] (GP) where they overlap at 400 nm. We therefore have to interpolate between Minton's value at 185 nm and GP's value at 400 nm. This interpolation is shown as a dashed line in Fig. 3. Here again, the behavior of liquid water (also plotted in Fig. 3) serves as a guide and as evidence that no electronic absorption features occur in the region of interpolation.

Essentially, we are taking Minton's measurements at 185 nm as evidence that m_{im} of ice is less than that of liquid water over most of the spectral region that has never been measured for ice. We put high priority on the measurement of the absorption coefficient of ice in this spectral region, because of its geophysical importance. The solar spectrum contains a large amount of energy in the 200–400-nm region, and most of the sunlight at 300–400 nm reaches the earth's surface, where it is important in the energy budgets of natural snow and ice surfaces.

For the 400–1400-nm region, we use the measurements of GP. They supersede the values of Luck[29] which had been recommended by Irvine and Pollack[1] for 1100–1400 nm.

IV. Near-Infrared, 1.4–2.8 μm

A. Sources of Data

In the 1.4–2.8-μm spectral region ice has an absorption coefficient that is too small to affect reflection measurements, yet it is large enough that very thin samples (a few hundred μm) must be used to obtain measurable transmission.

Reding[30] (1951) placed liquid water between two AgCl windows, froze it, and cooled it to T = −78°C. It was therefore polycrystalline and probably not bubble-free. Two samples were measured, but the 48-μm thick sample was unusable because of excessive scattering of light by cracks and bubbles. For the useful sample, the separation was 250 μm when the liquid was

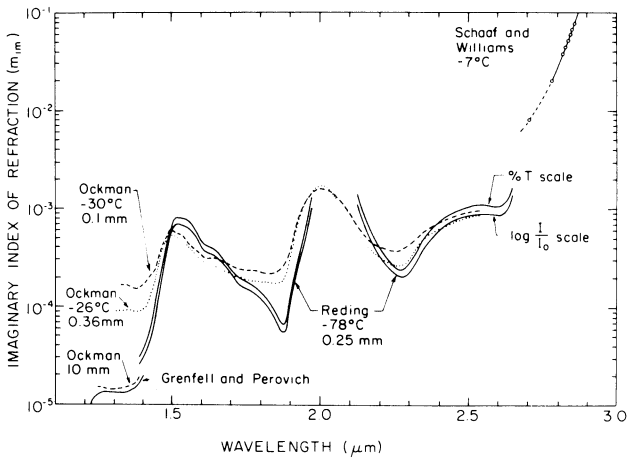

Fig. 4. Imaginary refractive index of ice in the near-infrared. Our compilation uses Ockman's[32] 0.1-mm sample for 1.45–1.61 μm and 1.89–2.11 μm, Reding's[30] values (frequency shifted as described in the text) for 1.61–1.89 μm and 2.11–2.62 μm. Straight lines are used to join from measurements of Grenfell and Perovich[12] at 1.4 μm to those of Ockman at 1.45 μm, and from those of Reding at 2.62 μm to those of Schaaf and Williams[10] at 2.78 μm.

poured in, but expansion during freezing may have increased the separation between the plates. The ordinate on Reding's Fig. 16 is labeled with both percent transmission and $\log(I/I_0)$, but the two scales are mutually inconsistent. Values of m_{im} derived using both scales are plotted here in Fig. 4. They differ by ~20%. Reding (personal communication, 1983) does not know which is correct, but favors the percent-transmission scale, which agrees with the reproduction of his spectrum in Fig. 3 of the paper by Hornig *et al.*[31] In their review article, Irvine and Pollack[1] apparently assumed the opposite.

No mention was made of a correction for reflection at the interfaces. A neglect of this correction would cause m_{im} to be underestimated, because less reflection occurs at an ice–AgCl interface than at an air–AgCl interface. By contrast, the other sources of error (scattering by bubbles, and increased separation of windows during freezing) would cause m_{im} to be overestimated. These errors may be much larger than the 20% uncertainty due to Reding's mislabeling of the axes.

Ockman[32] (1957) grew single crystals of hexagonal ice on a glass window and measured their spectra at −30°C and −178°C for 1.4–2.5 μm. There was almost no difference in the absorption for light polarized parallel and perpendicular to the *c* axis; we take the average of the two. There was, however, a substantial effect of temperature. As the temperature drops from −30°C to −178°C, the spectrum is shifted to longer wavelengths and has more structure and sharper peaks. A subsidiary minimum and maximum found by Ockman around 1.65 μm only at the colder temperature has also been observed in the reflectance spectra of laboratory frosts[33,34] to disappear at higher temperature.

Ockman measured his sample thickness more accurately than did Reding. For 1.4–2.5 μm, Ockman used three samples of thickness 102, 287, and 358 μm (uncertainty in thickness 3–5%) but only the spectrum of the thinnest sample was plotted in Ockman's[32] Fig. 17 and in Fig. 5 of his subsequent paper.[35] This is unfortunate, because (as IP pointed out) absorption measurements become inaccurate when transmission exceeds ~80%, since any random experimental errors, as well as a systematic neglect of reflection at the ice–window interfaces, lead to larger errors in m_{im} when the transmission is large. This is because $|\delta k_{abs}/k_{abs}| \simeq |\delta T/T|/|\ln T|$, where $\delta k_{abs}/k_{abs}$ is the relative error in k_{abs}, and $\delta T/T$ is the relative error in transmission T, so for $T > 0.8$, $|\delta k_{abs}/k_{abs}| > 5|\delta T/T|$. However, Ockman (personal communication, 1983) was able to provide us a graph of the absorption spectrum of the thickest crystal (358 μm) which had been omitted from his thesis. We have converted those values to m_{im} and ploted them in Fig. 4. The exaggeration of m_{im} in regions of large transmission is evident in Fig. 4, especially at 1.35 μm where the measurements overlap those of a thicker sample used at lower wavelength. Only the thickest (10-mm) sample gives accurate values of m_{im} here. We thus suspect that the values of m_{im} we derive from Ockman's transmissions may be excessive.

Ockman's plots of k_{abs} were obtained simply by using the relation $I = I_0 \exp(-k_{abs}d)$, where I is the measured intensity, I_0 that of the blank cell, and d is the sample thickness. He was only interested in obtaining the strengths of the band maxima, where the errors in background level do not have severe consequences. In principle, a correction for the reflection at interfaces should be applied to his measurements, if we could know how to do it. The blank had two air–glass interfaces. The sample had instead two ice–glass interfaces, if the ice was in contact with the glass. If not, there would have been two glass–air interfaces and two air–ice interfaces. Ockman thinks that the former situation is likely for the high-temperature (−29°C) results we are using, and that the ice became separated from the glass only upon cooling to −178°C for the low-temperature measurements. But if ice were in contact with glass, the reflection losses in the sample would be less than in the blank, because m_{re} of glass is closer to that of ice than to that of air. So the fact that substantial differences were observed among samples in the weakly absorbing parts of the spectrum means that there must have been losses from cracks or from unexpected air–ice interfaces. These cracks and interfaces can reduce the transmission by 15%, judging by comparison of the 0.1-mm sample with the 1-mm sample at 1.35 μm (compare Fig. 5 and 6 of Ockman[35]). The losses due to scattering or unexpected interfaces thus more than offset the difference in known interface reflections between sample and blank, so we choose not to correct for those reflections. The obvious presence of scattering in these measurements suggests that we should always take the lowest values of m_{im}, whenever two samples disagree. It appears (Fig. 4) that the thicker (358-μm) sample is more reliable.

B. Compilation of Imaginary Index

Our compilation in this region will be uncertain to about a factor of 2. This is a region that needs to be remeasured carefully at temperatures near 0°C with the aim of establishing quantitative values rather than just the location of peaks and shoulders.

The rationale for our choices is that

(a) transmission measurements give inaccurate values of m_{im} when transmission exceeds ~80%;

(b) the spectrum shifts to shorter wavelength as the temperature is raised; and

(c) Ockman's[32] measurements were apparently made more carefully than Reding's.[30]

Irvine and Pollack[1] used Reding's data everywhere except in his data-gap between 1.97 and 2.13 μm, because Reding had used a thicker sample than the one Ockman published. They estimated temperature corrections from Ockman's measurements at two temperatures. Our approach is to use Ockman's data for the 0.1-mm sample with no correction (i.e., to assume no temperature dependence between −30°C and −7°C) except in the regions where his transmission exceeded 80%. Ockman's results are generally to be preferred because he made them at temperatures close to the

melting point, and knew his sample thicknesses more accurately.

We join the values of Grenfell and Perovich[12] at 1.4 μm to those of Ockman at 1.45 μm with a smooth curve ($\ln m_{im}$ approximately linear in λ). We use Ockman's values uncorrected from 1.45 to 1.61 μm. From 1.61 to 1.89 μm we use Reding's values, shifted to shorter wavelength by ~0.05 μm and with the minimum at 1.85 μm broadened as Irvine and Pollack[1] did, because the minimum should not be so sharp at higher temperature. We use Ockman's data from 1.89 to 2.11 μm. From 2.11 to 2.62 μm we use Reding's data, shifted ~0.03 μm to shorter wavelength, based on the position of the minimum near 2.3 μm. [Where we use Reding's values, we take the log (I/I_0) scale. Although the % T-scale seems more likely to be correct, we prefer to take the lower m_{im} values to compensate partially for the scattering.] Finally, we draw a straight line (assuming $\ln m_{im}$ linear in λ) from Reding's (temperature-shifted) value at 2.62 μm to that of Schaaf and Williams[10] (−7°C) at 2.78 μm. This compilation is uncertain to about a factor of 2, judging from Fig. 4.

Ockman supplied the plot of the spectrum from the thicker (358-μm) sample after the compilation in this paper had been completed. In the regions where we are using Ockman's measurements, the differences between samples are judged not to be large enough to warrant redoing the compilation, in view of the large uncertainties in the measurements when m_{im} is small. The spectrum of the thicker sample (plotted in Fig. 4) suggests, however, that our compilation of m_{im} is probably as much as 15% too high from 1.44 μm to 1.63 μm, because we used the 0.10-mm sample.

This compilation is somewhat different from that given by Wiscombe and Warren.[5] They simply took Irvine and Pollack's[1] recommendation and applied the suggested temperature correction to −7°C.

V. Middle Infrared, 2.8–33 μm

Schaaf and Williams[10] (1973) measured the reflection spectrum of ice at −7°C formed by freezing of liquid water, so it was undoubtedly polycrystalline. They used the Kramers-Kronig analysis to obtain m_{re} and m_{im}. This method does not give m_{im} accurately when $m_{im} \ll m_{re}$, so their values of m_{im} are inaccurate for $\lambda < 2.78$ μm (dashed line in Fig. 4), and also at 3.5–4.3 μm where the uncertainty is ~50%. To do the Kramers-Kronig analysis they needed values of m_{im} in the far-infrared ($\lambda > 33$ μm) which were available only at 100 K. They tried to do a temperature correction on the far-infrared data to estimate values at −7°C, so there is some uncertainty in their values of m because of this, especially at the long-wavelength end near 33 μm where contributions to the Kramers-Kronig integral from outside the measured region become appreciable. Schaaf and Williams's reflectivity measurements can be reinterpreted in the future if far-infrared absorption spectra become available for ice near the melting point.

We use Schaaf and Williams's m_{im} values as given for 2.8–33 μm. Subsequent measurements[36,37] of the 3-μm band have been made only at much lower temperatures (<180 K).

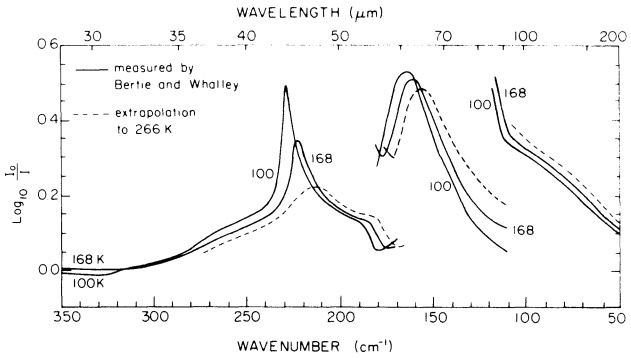

Fig. 5. Solid lines, transmission measurements for three ice films of unknown thickness, made at the two temperatures 100 K and 168 K (from Fig. 2 of Bertie and Whalley[38]). Dashed lines, our subjective guess of the spectrum at 266 K, using the solid lines as a guide.

VI. Far-Infrared, 33 μm–1.25 mm

A. Sources of Data

Bertie and Whalley[38] (1967) (BW) measured transmission through thin films of ice in the 360–50-cm^{-1} wave number region (28–200-μm wavelength). Their samples of hexagonal ice were prepared by condensing water vapor onto a polyethylene window at T = 173 K. Three samples of unknown thickness were used, each at two temperatures 100 and 168 K. The spectra, plotted in their Fig. 2, are reproduced here (with additions) as Fig. 5. There are substantial differences in the spectrum at the two temperatures. The temperatures were uncertain to ±20 K (D. Klug, personal communication, 1982). BW made no correction for reflection at the interfaces. Because the thicknesses were not known, we use these data only to estimate a temperature correction, not to obtain absolute values of m_{im}. BW (their Fig. 3) also showed that the spectrum of ice Ic is identical to that of ice Ih in this spectral region. They also showed that the two strong absorption bands (at 229 and 163 cm^{-1}) are both due to lattice vibrations. Amorphous ice, by contrast, lacks the structure shown in Fig. 5 and has only a single broad peak, as is also shown in Fig. 2 of Leger *et al.*[39] Because these absorption bands are due to lattice vibrations, they are completely absent in water vapor.

Bertie, Labbé and Whalley[11] (1969) (BLW) measured transmittance, at T = 100 K only, through thin films of ice Ih of a variety of thicknesses, using the same techniques as had Bertie and Whalley.[38] Several of the films were <1 μm thick. They reported values for the optical constants which were based on an indirect estimate of sample thickness. The main aim of the work was to determine the origin of the infrared polarizability which is responsible for the difference, Δm_{re}, of 0.47 between the microwave and visible refractive indices. By performing the Kramers-Kronig integral (2) over their observed absorbances, they computed the sample thickness which yielded the correct Δm_{re}. [Sample thickness enters in the computation of $k_{abs}(\nu)$.] This

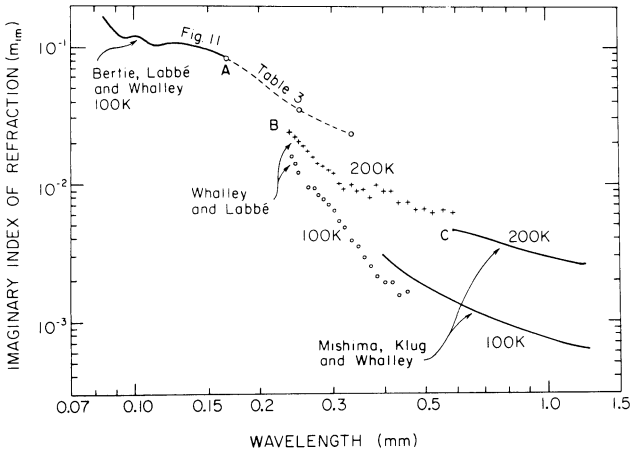

Fig. 6. Imaginary refractive index of ice in the transition from the strongly absorbing far-infrared region to the weakly absorbing microwave region. Our compilation for $T = -60°C$ joins point A to point B and follows the 200 K measurements of Whalley and Labbé[40] to point C.

sample thickness was further verified by comparing the derived value of k_{abs} at $\lambda = 2$ μm with that measured earlier by Ockman.[32] The thicknesses of the various samples were then obtained by scaling them in regions where their spectra overlapped.

These authors did not correct their absorption measurements for reflection at the interfaces. They assumed that the reduction in transmission was due entirely to absorption (after subtracting the spectrum of the empty cell), computed $m_{im}(\lambda)$, and used a Kramers-Kronig relation to obtain $m_{re}(\lambda)$. They recognized that this procedure leads to some error, the worst case being a neglect of ~27% reflection at $\nu = 229$ cm^{-1}. As they stated, this "undoubtedly means that the absorptivity and hence the reflectivity are overestimated by an uncertain amount in this region." They properly should have used an iterative procedure, computing reflection from m, then recomputing m, etc., until achieving self-consistency. Because the uncertainty in our procedure for correcting the 100 K data of BLW to 266 K is much larger than the error due to neglect of reflection by BLW, we have not reinterpreted BLW's transmission measurements for the present compilation.

BLW reported m_{re} and m_{im} for ice at $T = 100$ K in the 4000–60-cm^{-1} wave number region (2.5–167-μm wavelength). They also obtained some "preliminary and not very accurate" measurements of a 1-mm sample for 60–30 cm^{-1}. This long-wavelength end of their results is shown here as the dashed line in Fig. 6.

Their conclusion regarding Δm_{re} (microwave–visible) was that 74% of the difference was due to the translational bands in the far-infrared; 15% to the hindered-rotation band at 12 μm, and 7% to the 3-μm OH-stretching band. We use this information in Sec. VIII below as a guide to adjusting our temperature correction in the far-infrared.

Whalley and Labbé[40] (1969) (WL) grew blocks of ice of unspecified thickness by freezing liquid water (presumably hexagonal polycrystalline ice). They measured the absorption spectrum from 42 to 17 cm^{-1} at both 100 K and 200 K. These measurements are plotted in Fig. 6. They supersede the preliminary measurements of BLW[11] where they overlap them, because BLW's 1-mm thick ice block was too thin for accurate absorption measurements at $\nu = 30$ cm^{-1}. The absorption coefficient was expected (theoretically) to be proportional to ν^4 around $\nu = 40$ cm^{-1}, changing to a ν^2 dependence at longer wavelength. Within experimental error, the data (Fig. 1 of WL) support this.

Mishima, Klug, and Whalley[8] (1983) (MKW) used single crystals of ice Ih to extend the results of WL to 1.25-mm wavelength at four temperatures (80, 100, 150, 200 K). The absorptivity for polarized light was independent of the orientation of the single crystal. The values of m_{im} for 100 and 200 K are plotted in Fig. 6. MKW found the absorption to continue its decrease with approximately the expected ν^2 dependence. Under this assumption, the extrapolation of m_{im} for $T = 200$ K to $\lambda > 1.25$ mm agrees with microwave measurements cited below at $\lambda = 110$ mm and $T = 213$ K.

B. Compilation of Imaginary Index

Our source of m_{im} for 33–167 μm is BLW.[11] Their measurements at 100 K must be corrected to 266 K for our use, because no measurements are available near the melting point. Our procedure for estimating a temperature correction is somewhat arbitrary. We use the relative measurements of BW[38] at 100 and 168 K (±20 K) to estimate the temperature dependence. We note that the peaks become less sharp and shift to longer wavelength as the temperature increases. Using these two plots as a guide, we draw a subjective guess of the spectrum at 266 K, assuming these processes of broadening and wavelength shift to continue linearly with temperature (dashed line in Fig. 5). The temperature correction is then derived as the ratio of the 266 K plot to the 100 K plot. The ratio does not agree among samples where the spectra of two samples overlap. In these overlap regions, we choose the sample that gave a temperature correction closest to 1.0. This correction factor is plotted in Fig. 7. It is also constrained to make BLW's m_{im} at 300 cm^{-1} agree, after correction, with that measured by Schaaf and Williams[10] at 266 K (Fig. 8). The correction is applied to the m_{im} of BLW; the result is shown as the dashed line in Fig. 9. By this procedure, the 229-cm^{-1} peak at 100 K moves to 209 cm^{-1}, somewhat further than the 214 cm^{-1} expected from measurements of the peak position published in Fig. 4 of Zimmermann and Pimentel.[41] This is our initial guess of m_{im}. In Sec. VIII below we will adjust the peak position to 214 cm^{-1} and then slightly adjust the magnitude of m_{im} in order to match the known Δm_{re} (microwave–visible), obtaining finally the dotted line in Fig. 9.

We assume that no temperature correction is necessary at $\nu = 60$ cm^{-1} ($\lambda = 167$ μm). This is suggested by Fig. 6, where the 200 K and 100 K plots of WL[40] are seen to converge toward an extrapolated meeting point at 60 cm^{-1} (point A) which also agrees with BLW's measured

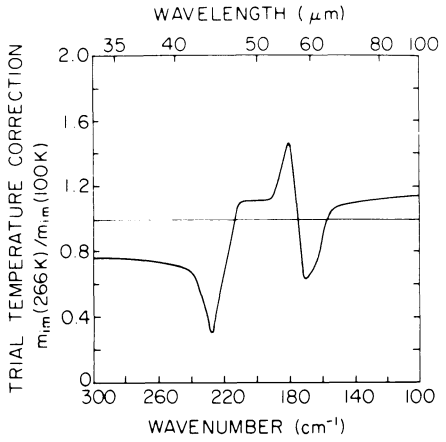

Fig. 7. Initial temperature correction which was applied to the 100 K data of Bertie *et al.*,[11] to obtain values of m_{im} for 266 K. It is derived from the 266 K and 100 K curves of Fig. 5. This temperature correction was later refined during the Kramers-Kronig analysis.

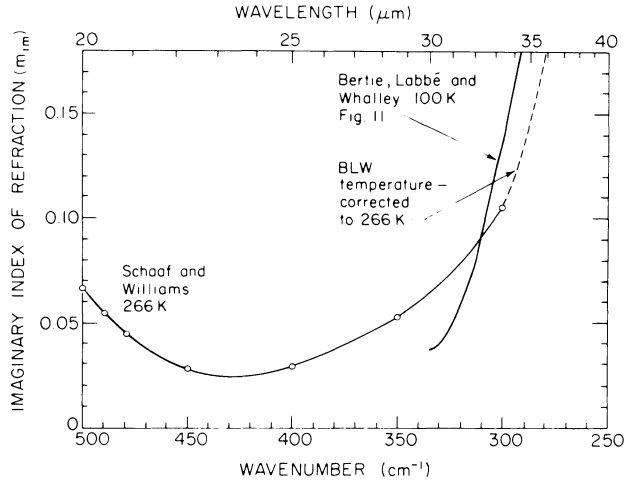

Fig. 8. Imaginary refractive index of ice near $\lambda = 33$ μm. This is where Schaaf and Williams's[10] data must be joined to the (temperature-corrected) data of Bertie *et al.*[11]

m_{im} there. The interpolation between the temperature-corrected m_{im} at 100 cm^{-1} and the measured m_{im} at 60 cm^{-1} (Fig. 9) ignores the wiggles seen in the data in this region, on the assumption that they would be broadened and smoothed at higher temperature.

For $\lambda > 167$ μm the temperature dependence of m_{im} becomes appreciable even near the melting point. Our compilation for $T = -60$°C connects point A (BLW) in Fig. 6 with point B (WL, 200 K). A smooth curve is drawn through the data of WL to meet point C of MKW at $T = 200$ K. The m_{im} at higher temperatures for 60–33 cm^{-1} are obtained by using the difference between the 100 K and 200 K measurements, and extrapolating with the assumption that m_{im} is linear in temperature. This is suggested by the fact that over the entire 42–17-cm^{-1} region, m_{im} (200 K) $\simeq m_{im}$ (100 K) + 0.006. Beyond 33 cm^{-1} (300 μm), the extrapolation into the microwave region is described below.

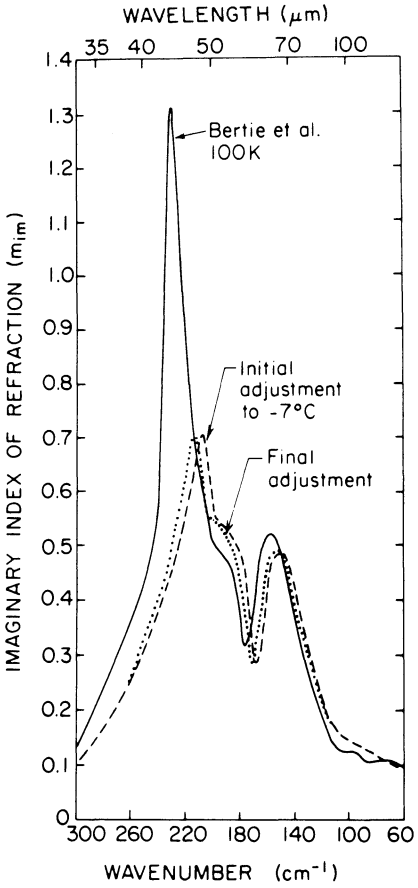

Fig. 9. Imaginary refractive index of ice in the far-infrared. Solid line, data for 100 K from Bertie *et al.*[11] Dashed line, values adjusted to −7°C by the function shown in Fig. 7. Dotted line, refined adjustment to −7°C as described in Sec. VIII of the text.

VII. Microwave and Radiowave, 1 mm–8.6 m

A. Sources of Data

Most of these data are plotted in Fig. 10.

Lamb[42] (1946) measured loss tangent at $\lambda = 30$ mm, as a function of temperature from −1°C to −50°C. (Lamb's value at −1°C is reproduced incorrectly, a factor of 3 too low, in Fig. 7 of Evans's review.[2])

Lamb and Turney[43] (1949) grew ice from distilled water. They corrected Lamb's[42] value of ε' but not his tanδ at $\lambda = 30$ mm. They reported new measurements of tanδ at $\lambda = 12.5$ mm, for temperatures from 93 to 273 K.

Cumming[44] (1952) measured loss tangent at $\lambda = 32$ mm, at temperatures from 0° to −18°C, with a precision of better than 5%. Ice grown from three sources (distilled water, tap water, and melted snow) all gave the same loss tangent. Cumming confirmed his intrument's calibration by obtaining good agreement with the known loss tangent of other materials.

Perry and Straiton[45] (1973) obtained corrected values of ε' and ε'' at −28°C, $\lambda = 3.1$ mm, after Gough[46] pointed out that they had earlier[47] reported a wrong value of ε' (1.9 instead of 3.2).

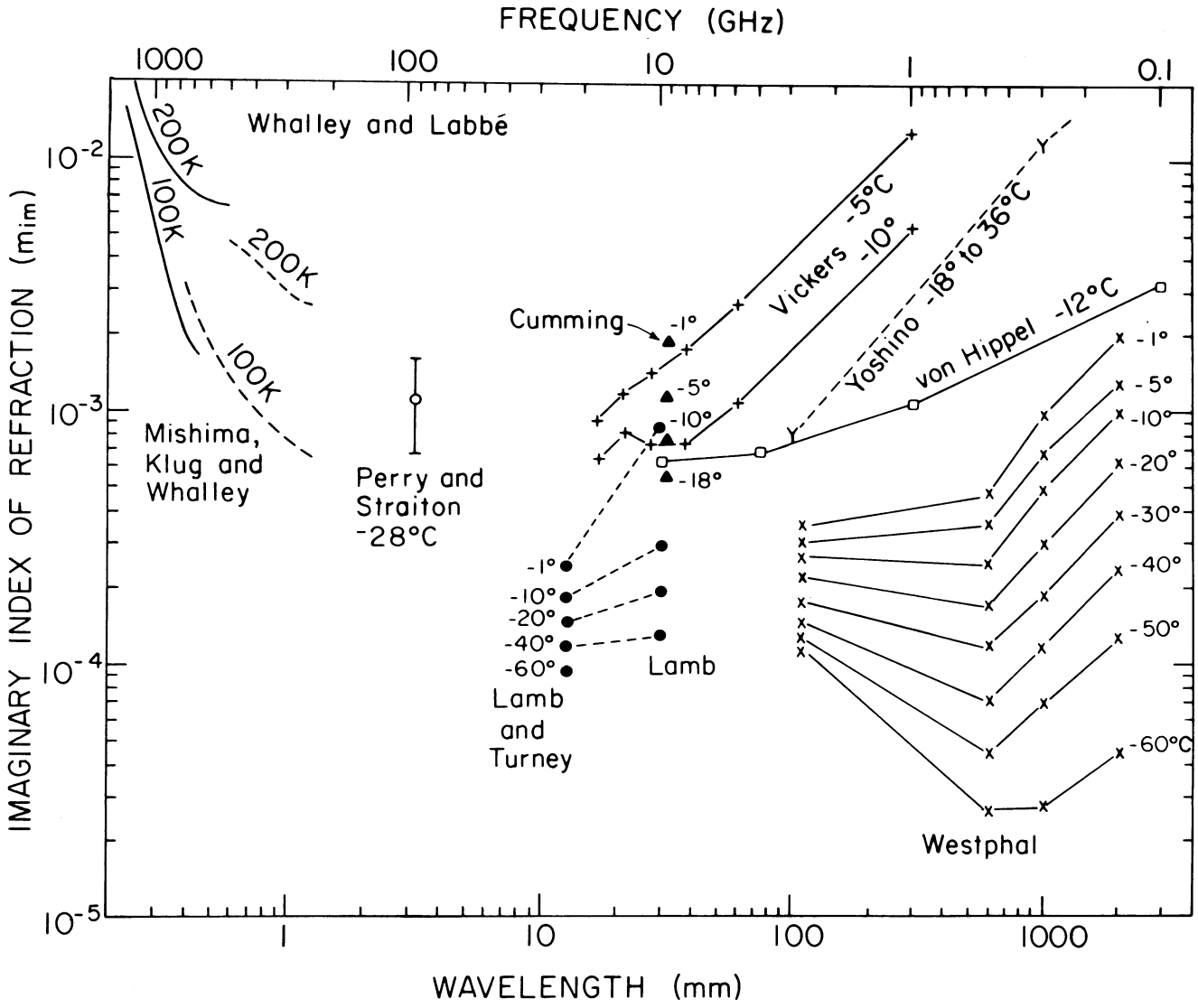

Fig. 10. Imaginary index of refraction of ice in the microwave and radiowave regions, according to various investigators. For $\lambda > 2$ mm, measurements were made only at the points marked by symbols; they are connected here by lines only for display purposes. An error bar shows the uncertainty quoted by Perry and Straiton.[45]

Vant *et al.*[48] (1974) estimated $\tan\delta$ at $\lambda = 30$ mm to be "of the order of 20×10^{-4} (0°C to −35°C)," giving $m_{im} \simeq 2 \times 10^{-3}$, i.e., between Cumming's −1°C and −5°C values. They also reported a loss tangent of 0.001 ± 0.001 at −35°C which seems to apply to a frequency of 35 GHz ($\lambda = 8.6$ mm), although their discussion does not make this clear. The corresponding m_{im} is 9×10^{-4}. This is not inconsistent with our compilation but is too uncertain to be of any use to us.

Westphal (unpublished) measured loss tangent of natural glacier ice from three locations, for temperatures from −1°C to −60°C and frequencies from 150 MHz to 2.7 GHz (2-m–111-mm wavelength. The measurements were reviewed by Evans[2] and tabulated by Jiracek.[17] (Jiracek pointed out that the earlier presentation of Westphal's data by Ragle *et al.*[49] was incorrect because of lack of a multiplier.) Westphal found that annealing the ice at −10°C for a few hours resulted in lower losses, so the results were reported for the annealed samples. Two of the three ice samples gave identical values of $\tan\delta$, which are plotted here in Fig. 10. They had densities of 0.898 and 0.902, in comparison with pure ice density of 0.917, so they did contain a small amount of air. Westphal estimated that his measurements of $\tan\delta$ were accurate to 20%.

Vickers[50] (1977) reported decibel-power-loss (dB), which can be converted to m_{im}, for bubble-free lake ice, $17 \leqslant \lambda \leqslant 300$ mm, at −5°, −10°, and −15°C. Although the data are in tolerable agreement with Cumming[44] and von Hippel[51] at $\lambda = 32$ mm, they show a trend of m_{im} increasing with λ (Fig. 10) which leads to gross disagreement with Westphal at $\lambda > 110$ mm. The reason may be that the dielectric losses were barely detectable by Vickers, and he may have been reporting constant instrument noise which would lead to an ap-

parent increase of m_{im} with λ when dB is converted to m_{im}.

von Hippel[51] (1945, p. 220) reported ε' and $\tan\delta$ for ice at $-12°C$, 30 mm $\leqslant \lambda \leqslant$ 3 km. Evans[2] pointed out that von Hippel's ε' was in error, rising from 3.2 at λ = 30 mm to 4.2 at λ = 300 m, whereas it should remain constant at $\varepsilon' = 3.2$ in this spectral region. We deduce m_{im} (shown in Fig. 10) from the reported loss tangent by use of a constant $\varepsilon' = 3.2$ instead of von Hippel's ε', but since von Hippel's ε' was in error we suppose his $\tan\delta$ may also have been in error.

Yoshino[52] (1961) measured ε' and $\tan\delta$ in glacier ice, from $-18°$ to $-36°C$, 100 mm $\leqslant \lambda \leqslant$ 200 m. They were reviewed and rejected by Evans[2] in comparison with smaller values of other authors because "any unforeseen errors in the experimental technique may increase the losses but they cannot in any circumstances be expected to result in measured loss less than the true value." The same statement applies to the values from von Hippel.

Johari and Charette[53] (1975) measured ε' and $\tan\delta$ at six temperatures in the range from $-1°$ to $-25°C$, at 5 and 8.6-m wavelength.

Johari[54] (1976) reported ε' and ε'' for ice at $-5°C$, 3 $\leqslant \lambda \leqslant$ 600 m. The measurements of ε'' match those of Westphal at λ = 3 m.

B. Compilation of Imaginary Index

We use data from Mishima *et al.*,[8] Cumming,[44] Westphal (as tabulated by Jiracek[17]), Johari and Charette,[53] and Johari.[54] All other measurements are ignored, as discussed below.

1. *300 μm–111 mm*

For the $-60°C$ values, we use the 200 K measurements of WL[40] and MKW[8] as far as 1.25 mm, then interpolate (assuming $\ln m_{im}$ proportional to $\ln\lambda$) to Westphal's[17] value at $-60°C$ at λ = 111 mm. For the higher temperatures (-1, -5, $-20°C$) we start with the values we obtained at λ = 300 μm by extrapolation from the 100 K and 200 K data of WL[40] as described in Sec. VI.B. We then interpolate from these values, through Cumming's[44] values at λ = 32 mm, to Westphal's measurements at λ = 111 mm.

There are several other conflicting sets of measurements in this region. Let us consider them in turn.

Perry and Straiton[45] gave a value of m_{im} at λ = 3.2 mm, $T = -28°C$ which looks realistic, but we choose to ignore it because of severe doubts about the accuracy of their experimental technique.[46]

Lamb[42] measured m_{im} (T) at λ = 30 mm; Lamb and Turney[43] at λ = 12.5 mm. These are lower by a factor of ~2.5 than Cumming's[44] measurements at 32 mm. It is difficult to choose between the results of Cumming and Lamb. Evans[2] stated that errors can only lead to higher reported m_{im}, which means that Lamb should be favored. However, Cumming's measurements seem to have been made more carefully (Johari, personal communication, 1981). Furthermore, because of the general trend of m_{im} with λ here, it is very unlikely that the measurements of Lamb and Turney and of Lamb can both be correct. Here we choose to ignore both of them, and to use Cumming's values. However, on theoretical grounds there is no reason to expect anything other than the frequency-squared dependence of k_{abs} through this spectral region.[8] Our interpolation for $-60°C$ agrees generally with the frequency-squared dependence, but at the higher temperatures our compilation deviates from the theoretical relation because we choose to believe the measurements of Cumming.[44] (Cumming made no measurements below $-18°C$.) It is clear that more measurements are needed in this spectral region, which is of great interest for microwave remote sensing. Measurements in this low-loss spectral region are difficult because transmission methods require long samples, and cavity-resonance methods require cavity dimensions as small as the wavelength (F. Ulaby, personal communication, 1983).

The measurements of Vickers[50] and Yoshino[52] are probably too high, as discussed above. Cumming's values are in agreement with those of von Hippel[51] (1954), but just at the one wavelength λ = 30 mm. von Hippel measured m_{im} to increase monotonically as λ increases from 30 mm to 3 km, with values as much as a factor of 7 higher than Westphal's.[17] Since von Hippel's $m_{re}(\lambda)$ is in error at $\lambda >$ 30 mm (compare Fig. 6 of Evans[2]), we tend to doubt his m_{im} values as well, and prefer those of Westphal.

Although there are no reliable measurements of m_{im} between 1.25 and 32 mm, we can be sure that there is no strong absorption band in the unmeasured region, because the infrared absorption bands fully account for the measured microwave m_{re}.[11,16] This is also substantiated by the qualitative observation of Champion and Sievers[55] that ice is "completely transparent" at λ = 2.5 mm.

2. *111 mm–8.6 m*

For 111 mm–2 m we use Westphal's data from Ward Hunt Island Glacial Ice (Table II of Jiracek[17]). The results were the same in Tuto Tunnel, Greenland, but were generally higher at Little America V. We follow Evans's[2] recommendation and use the lower values.

For 2.0–8.6 m we use Johari and Charette's[53] data at temperatures -1, -5, and $-20°C$. For $-60°C$ we extrapolate Westphal's plot.

Beyond 8.6 m, Johari[54] has measured m_{im} out to 600 m, but only at $-5°C$. The temperature dependence becomes extreme in this region, so we stop our compilation at 8.6 m. The longer wavelengths have also been adequately covered in other review articles.

VIII. Adjustment of Far-Infrared Absorption Spectrum

We now refine our temperature correction to m_{im} in the far-infrared until we obtain the correct difference between visible and microwave real indices, using the Kramers-Kronig relations.

A. Real-Index-of-Refraction Reference Points

The real index can be measured independently of the imaginary index if $m_{im} \ll m_{re}$. The real index is well

established in the two regions of the spectrum where the absorption is very small: visible and microwave.

We use the refractive index reported at $\lambda = 589$ nm by Merwin.[15] Ice is very slightly birefringent; $m_{re} = 1.3090$ for the ordinary ray, and 1.3140 for the extraordinary ray. These values differ by only one part per thousand, and we simply average them to obtain $m_{re} = 1.3097$ for polycrystalline ice.

The real refractive index is constant over a large region of the microwave and radiowave spectrum and is the square root of the limiting high-frequency permittivity ε_∞. Gough[16] has measured ε' for ice Ih from $T = 2$ K to 270 K at frequencies up to 1 MHz, extrapolating to ε_∞. His data were found to fit very well to a quadratic function of temperature:

$$\varepsilon_\infty = 3.093 + 0.72 \times 10^{-4} T + 0.11 \times 10^{-5} T^2.$$

This gives us $m_{re} = 1.7772$, 1.7837, 1.7865, and 1.7872 at our reference temperatures −60, −20, −5, and −1°C, respectively. We assume these to be valid at $\lambda = 200$ mm. This slight temperature dependence is due to the temperature dependence of the far-infrared absorption spectrum. For the Kramers-Kronig analysis we use the value for −7°C, $m_{re} = 1.7861$. This gives us a difference between the two real indices, $\Delta m_{re} = 0.4764$.

B. Refinement of Temperature Correction

The temperature correction which was guessed by extrapolating from Bertie and Whalley's[38] low-temperature measurements in Fig. 5 must be refined in two ways. First, our initial temperature correction gave a peak at $\nu = 209$ cm^{-1}. Although values of m_{im} have not been measured at high temperature, the position of the peak is known as a function of temperature as given by Zimmerman and Pimentel.[41] They show the peak value at $\nu = 214$ cm^{-1} for $T = -7$°C. Second, when we perform the Kramers-Kronig integral (2) to obtain Δm_{re}, we obtain Δm_{re} slightly (<1%) different from the correct measured value of 0.4764.

Our procedure is first to shift the absorption spectrum to higher frequency so that the peak position comes to 214 cm^{-1}, and second to raise m_{im} until we obtain the correct Δm_{re}. These adjustments are both applied only for $100 \leqslant \nu \leqslant 300$ cm^{-1}, with maximum adjustment at 200 cm^{-1} and no adjustment at 100 or 300 cm^{-1}. The adjustment is further refined during the complete analysis of $m_{re}(\lambda)$ described in Sec. IX below, resulting in the dotted line in Fig. 9.

IX. Computation of Real Index

We compute $m_{re}(\lambda)$ from $m_{im}(\lambda)$ using two different methods and obtain identical results at all wavelengths with both methods. The first method is the Kramers-Kronig (KK) integral used by Downing and Williams[56] and Bertie *et al.*[11];

$$m_{re}(\nu) = 1 + \frac{2}{\pi} P \int_0^\infty \frac{\nu'^2 m_{im}(\nu') - \nu\nu' m_{im}(\nu)}{\nu'^2 - \nu^2}\, d \ln\nu'. \quad (3)$$

This equation is equivalent to Eq. (1) but is more convenient for numerical computations because its singularity is of type 0/0.

The second method is the subtractive-Kramers-Kronig (SKK) integral recommended by Ahrenkiel[57] and by Bachrach and Brown,[58] used by Hale and Querry[14] in their compilation of liquid water refractive index:

$$m_{re}(\lambda_0) = m_{re}(\lambda_1) + \frac{2(\lambda_1^2 - \lambda_0^2)}{\pi} P \int_0^\infty \frac{\lambda^2 m_{im}(\lambda)}{(\lambda_0^2 - \lambda^2)(\lambda_1^2 - \lambda^2)}\, d \ln\lambda. \quad (4)$$

The SKK method requires specification of a known (measured) value of m_{re} at some wavelength λ_1 (we use $\lambda_1 = 0.5893$ μm) and is rather insensitive to m_{im} at wavelengths far removed from λ_0. It is thus the preferred method if m_{im} is known only in a short spectral region which is also the region of interest of m_{re}. For the case of ice, however, we do have sufficient knowledge of m_{im} over the entire spectrum to allow us to do the KK analysis almost as easily as the SKK analysis.

The KK integral (3) is done numerically (except at the singularity) using trapezoidal integration for 100,000 points equally spaced in logν. The results for m_{re} differ at most in the 5th decimal place if only 30,000 points are used. For each frequency ν, the integral over the singularity at $\nu' = \nu$ is done analytically between the two grid points $\nu' = \nu - s$ and $\nu' = \nu + t$, with m_{im} approximated as linear in ν between these two points: $m_{im} \simeq a + b\nu'$. This integral is

$$\frac{2}{\pi} P \int_{\nu-s}^{\nu+t} \frac{\nu'(a + b\nu') - \nu m_{im}(\nu)}{(\nu'^2 - \nu^2)}\, d\nu' = b(t + s) + \frac{1}{2}[a + m_{im}(\nu) - b\nu] \ln\left(\frac{2\nu + t}{2\nu - s}\right). \quad (5)$$

The singularity is of type 0/0, and the contribution of (5) to (3) is always negligible with the fine grid we use.

The integral in (3) runs from zero to infinity, so we must postulate m_{im} outside the measured range. Our computed m_{re} turns out to be very insensitive to how this assumption is made. For $\lambda > 8.6$ m we use m_{im} as given by Johari[54] for 8.6 m $\leqslant \lambda \leqslant$ 600 m, and by Ray[3] for $\lambda > 600$ m. For $\lambda < 45$ nm we extrapolate m_{im} from 45 nm linearly in λ to $m_{im} = 0$ at $\lambda = 33$ nm. A soft-x-ray absorption band is postulated in the 2.33–2.40-nm region, peaking at 2.36 nm, corresponding to the emission spectrum measured qualitatively by Gilberg *et al.*[59] for ice Ih and Ic. This also agrees more or less with the peak postulated for liquid water in Hale and Querry's[14] SKK analysis. We are unaware of any other absorption band between 2.4- and 45-nm wavelength. We first adjust the magnitude of this postulated x-ray band until we obtain the correct observed value of m_{re} in the visible, and then proceed to compute m_{re} at all wavelengths. As long as its amplitude is adjusted to obtain the correct visible m_{re}, the exact shape and location of this peak has no effect on $m_{re}(\lambda > 45$ nm) unless it is moved to considerably longer wavelength. If it is moved up to 24 nm, the ultraviolet m_{re} is altered by up to 0.06 at the short-wave end (45 nm), with negligible difference for $\lambda > 200$ nm. (The SKK analysis, which does not require an assumption about the x-ray band, gives the same m_{re} at 45 nm as does the KK analysis assuming the x-ray band

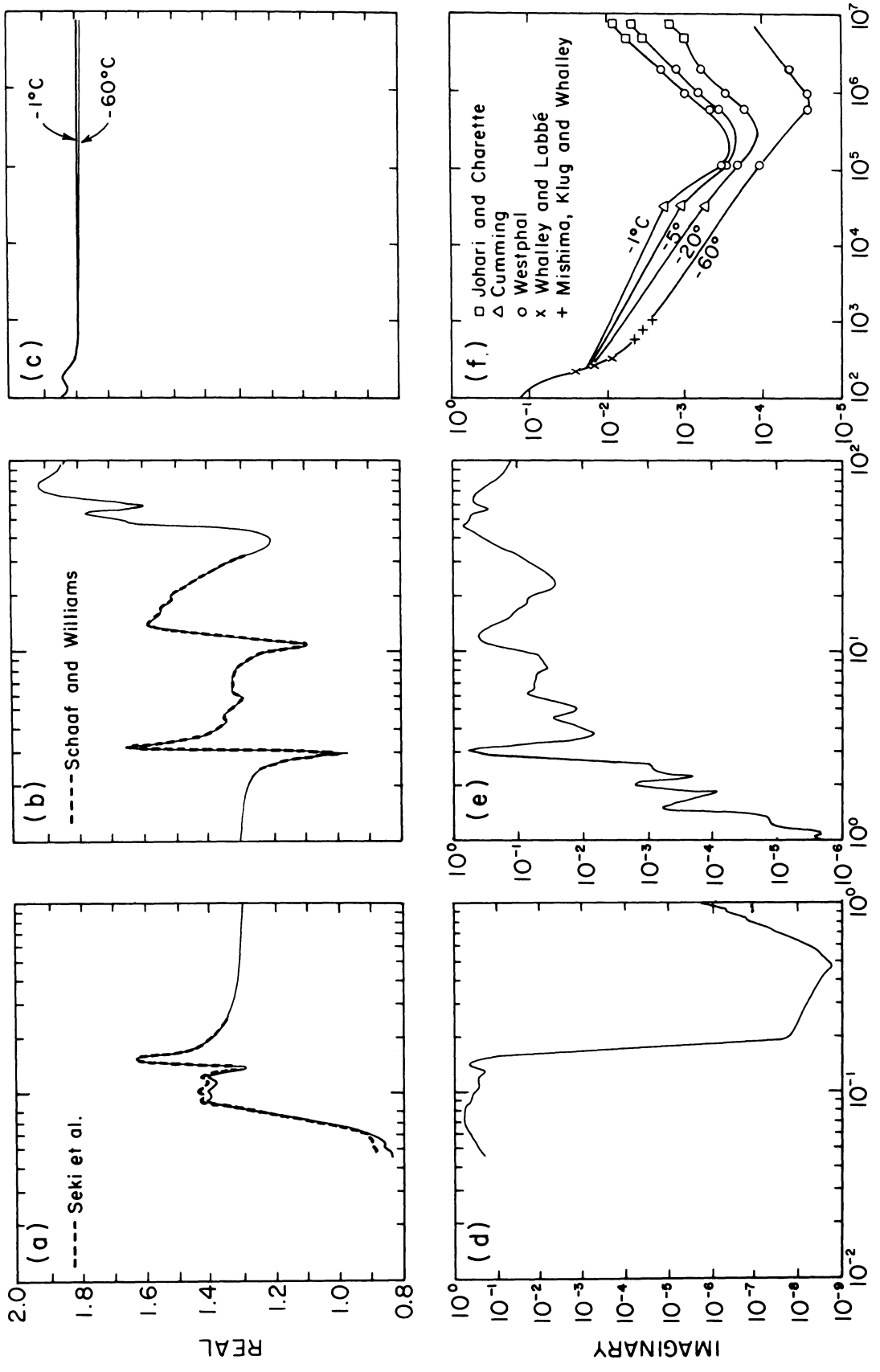

Fig. 11. Compilation of real (a)–(c) and imaginary (d)–(f) parts of the refractive index of ice Ih at $T = -7°C$ for $\lambda < 167$ μm and at four temperatures for $\lambda > 167$ μm. Data sources and uncertainties are discussed in the text. These graphs are tabulated in Tables I and II. The dashed line in (a) shows the results of Seki *et al.*[7] which differ from our compilation as discussed in Sec. IX of the text. The dashed line in (b) similarly shows the results of Schaaf and Williams.[10] In (f) the curves are a subjective interpolation between the data points shown.

at 2.36 nm.) The computed $m_{re}(\lambda)$ is shown in Fig. 11.

Seki *et al.*[7] performed a KK analysis to interpret their ultraviolet reflectance measurements, obtaining both m_{re} and m_{im}. They did not state what assumption they made for the soft-x-ray band. When we do the KK analysis with the above assumptions, we obtain slightly different values of m_{re} than they obtained, as shown in Fig. 11(a). This suggests that whatever Seki *et al.* assumed was equivalent to assuming a band centered at 8 nm instead of at 2.4 nm. The difference shown in Fig. 11(a) can thus be taken as the uncertainty in the ultraviolet m_{re} due to lack of knowledge of m_{im} for $\lambda < 45$ nm.

The same comparison can be done with Schaaf and Williams's[10] middle-infrared m_{re}, since they also made reflectance measurements and performed a KK analysis to interpret them. They had to assume a temperature correction for BLW's far-infrared measurements, as we have done, in order to obtain values of m_{im} outside their measured region. They did not state how they did this temperature correction. Comparison of their m_{re} with ours shows excellent agreement. The differences are smaller than the width of the line in Fig. 11(b). Apparently we have independently arrived at the same far-infrared temperature correction that Schaaf and Williams used.

We also test the sensitivity of our results to the termination point of our integration at long wavelength. Differences in m_{re} appear only at the longwave end of our compilation ($\lambda = 8.6$ m), in the 5th decimal place, if the integration in (3) is terminated at $\lambda < 10$ km. Our use of $\lambda = 1000$ km for the termination is therefore quite adequate.

The computation of m_{re} uses the -5°C values of m_{im} in the microwave. Our m_{re} is forced to agree with Gough's[16] value at $\lambda = 200$ mm. However, our calculation of m_{re} at longer wavelengths disagrees slightly (difference = 0.0015) with the measurement of Johari and Charette[53] at $\lambda = 5$ m, as shown in Fig. 12. This is also about the level of uncertainty of the measurement (Fig. 4 of Gough[16]; Fig. 2 of Johari and Charette[53]). The compilation for other temperatures is forced to pass through the values corresponding to the real part of the permittivity, ε', measured by Gough,[16] and to parallel the behavior of the -7° compilation at longer wavelengths, resulting in a lack of agreement with values of Johari and Charette.

The real index in the microwave depends slightly on temperature, as we show in Figs. 11(c) and 12, but we obtain this temperature dependence from measurements rather than computing it. This is because the temperature dependence of the microwave m_{re} is due to the temperature dependence of m_{im} not in the microwave but in the far-infrared[9,16] where $m_{im}(T)$ has not been measured near the melting point.

The fractional uncertainty in m_{re} is generally much smaller than that in m_{im}. The real index may be taken as accurate to within the width of the line in Figs. 11(a)–(c) for 200-nm–25-μm wavelength and for $\lambda > 300$ μm. The uncertainty in the far-ultraviolet, $\lambda < 200$ nm, may be taken as the difference between the dashed and solid lines in Fig. 11(a). It is at worst ~0.05 at $\lambda = 45$ nm. The only other spectral region where the uncertainty in m_{re} is much larger than the width of the line in Figs. 11(a)–(c) is in the far-infrared, ~25–300-μm wavelength. This is because the uncertainty in m_{im} between 33 and 167 μm (Fig. 9) will significantly affect m_{re} in a somewhat expanded region. New measurements near the melting point in the far-infrared would very likely alter our compilation of both m_{re} and m_{im} in that region.

The complete compilation of m_{re} and m_{im} is shown in Fig. 11 and tabulated in Tables I and II.

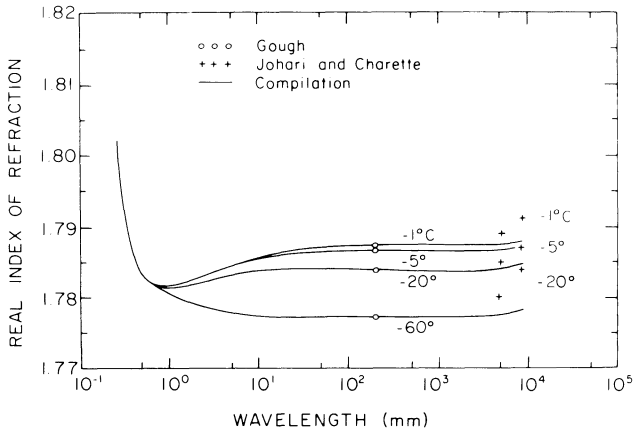

Fig. 12. Real index of refraction at microwave frequencies. The compilation is based on the Kramers-Kronig analysis at $T = -7$°C. The compilation for other temperatures is forced to pass through the values corresponding to the real part of the permittivity, ε', measured by Gough,[16] and to parallel the behavior of the -7° compilation at longer wavelengths, resulting in a lack of agreement with values of Johari and Charette. These curves are the same as those in Fig. 11(c) displayed here on an expanded scale.

X. Summary and Recommendation for Needed Measurements

A compilation of the complex refractive index of ice from the ultraviolet to the far-infrared has been made for temperature $T = -7$°C, and recommended for use at temperatures between -60°C and 0°C. A temperature-dependent refractive index is compiled for the microwave. Because of the uncertainties discussed above, these compilations may be considerably in error in some spectral regions. New measurements of the absorption coefficient of pure ice within 60 K of the melting point are needed in five wavelength regions:

Table I. Real (m_{re}) and imaginary (m_{im}) parts of the complex index of refraction of ice Ih at -7°C, from 45-nm to 167-μm wavelength (λ). Data sources are discussed in the text. These values are graphed in Fig. 11. Wavelengths were chosen for the tables in order adequately to resolve the variations in both real and imaginary index. For intermediate wavelengths not given in the table one should interpolate m_{re} linearly in logλ and logm_{im} linearly in logλ. Table I is on the next three pages.

$\lambda(\mu m)$	m_{re}	m_{im}	$\lambda(\mu m)$	m_{re}	m_{im}	$\lambda(\mu m)$	m_{re}	m_{im}
4.430E-2	0.8344	1.640E-1	1.393E-1	1.3203	3.440E-1	4.600E-1	1.3151	1.530E-9
4.510E-2	0.8368	1.730E-1	1.409E-1	1.3630	3.820E-1	4.700E-1	1.3145	1.550E-9
4.590E-2	0.8373	1.830E-1	1.425E-1	1.4187	4.010E-1	4.800E-1	1.3140	1.640E-9
4.680E-2	0.8377	1.950E-1	1.435E-1	1.4583	4.065E-1	4.900E-1	1.3135	1.780E-9
4.770E-2	0.8383	2.080E-1	1.442E-1	1.4903	4.050E-1	5.000E-1	1.3130	1.910E-9
4.860E-2	0.8404	2.230E-1	1.450E-1	1.5213	3.890E-1	5.100E-1	1.3126	2.140E-9
4.960E-2	0.8472	2.400E-1	1.459E-1	1.5538	3.770E-1	5.200E-1	1.3122	2.260E-9
5.060E-2	0.8552	2.500E-1	1.468E-1	1.5778	3.450E-1	5.300E-1	1.3118	2.540E-9
5.170E-2	0.8605	2.590E-1	1.476E-1	1.5964	3.320E-1	5.400E-1	1.3114	2.930E-9
5.280E-2	0.8625	2.680E-1	1.480E-1	1.6065	3.150E-1	5.500E-1	1.3110	3.110E-9
5.390E-2	0.8616	2.790E-1	1.485E-1	1.6117	2.980E-1	5.600E-1	1.3106	3.290E-9
5.510E-2	0.8609	2.970E-1	1.494E-1	1.6192	2.740E-1	5.700E-1	1.3103	3.520E-9
5.640E-2	0.8642	3.190E-1	1.512E-1	1.6252	2.280E-1	5.800E-1	1.3100	4.040E-9
5.770E-2	0.8692	3.400E-1	1.531E-1	1.6340	1.980E-1	5.900E-1	1.3097	4.880E-9
5.900E-2	0.8776	3.660E-1	1.540E-1	1.6369	1.720E-1	6.000E-1	1.3094	5.730E-9
6.050E-2	0.8930	3.920E-1	1.550E-1	1.6383	1.560E-1	6.100E-1	1.3091	6.890E-9
6.200E-2	0.9104	4.160E-1	1.569E-1	1.6372	1.100E-1	6.200E-1	1.3088	8.580E-9
6.360E-2	0.9309	4.400E-1	1.580E-1	1.6323	8.300E-2	6.300E-1	1.3085	1.040E-8
6.530E-2	0.9537	4.640E-1	1.589E-1	1.6222	5.800E-2	6.400E-1	1.3083	1.220E-8
6.700E-2	0.9819	4.920E-1	1.610E-1	1.5827	2.200E-2	6.500E-1	1.3080	1.430E-8
6.890E-2	1.0233	5.170E-1	1.625E-1	1.5564	1.000E-2	6.600E-1	1.3078	1.660E-8
7.080E-2	1.0673	5.280E-1	1.648E-1	1.5245	3.000E-3	6.700E-1	1.3076	1.890E-8
7.290E-2	1.1120	5.330E-1	1.669E-1	1.5032	1.000E-3	6.800E-1	1.3073	2.090E-8
7.380E-2	1.1313	5.340E-1	1.692E-1	1.4850	3.000E-4	6.900E-1	1.3071	2.400E-8
7.510E-2	1.1575	5.310E-1	1.713E-1	1.4723	1.000E-4	7.000E-1	1.3069	2.900E-8
7.750E-2	1.2004	5.240E-1	1.737E-1	1.4599	3.000E-5	7.100E-1	1.3067	3.440E-8
8.000E-2	1.2384	5.100E-1	1.757E-1	1.4511	1.000E-5	7.200E-1	1.3065	4.030E-8
8.270E-2	1.2732	5.000E-1	1.779E-1	1.4427	3.000E-6	7.300E-1	1.3062	4.300E-8
8.550E-2	1.3216	4.990E-1	1.802E-1	1.4350	1.000E-6	7.400E-1	1.3060	4.920E-8
8.860E-2	1.3896	4.680E-1	1.809E-1	1.4328	7.000E-7	7.500E-1	1.3058	5.870E-8
9.180E-2	1.4164	3.800E-1	1.821E-1	1.4292	4.000E-7	7.600E-1	1.3057	7.080E-8
9.300E-2	1.4091	3.600E-1	1.833E-1	1.4260	2.000E-7	7.700E-1	1.3055	8.580E-8
9.540E-2	1.4006	3.390E-1	1.843E-1	1.4232	1.000E-7	7.800E-1	1.3053	1.020E-7
9.920E-2	1.4017	3.180E-1	1.850E-1	1.4214	6.377E-8	7.900E-1	1.3051	1.180E-7
1.033E-1	1.4093	2.910E-1	1.860E-1	1.4190	3.750E-8	8.000E-1	1.3049	1.340E-7
1.078E-1	1.4022	2.510E-1	1.870E-1	1.4166	2.800E-8	8.100E-1	1.3047	1.400E-7
1.100E-1	1.3924	2.440E-1	1.880E-1	1.4143	2.400E-8	8.200E-1	1.3045	1.430E-7
1.127E-1	1.3842	2.390E-1	1.890E-1	1.4122	2.200E-8	8.300E-1	1.3044	1.450E-7
1.140E-1	1.3807	2.390E-1	1.900E-1	1.4101	1.900E-8	8.400E-1	1.3042	1.510E-7
1.181E-1	1.3819	2.440E-1	1.910E-1	1.4081	1.750E-8	8.500E-1	1.3040	1.830E-7
1.210E-1	1.3963	2.470E-1	1.930E-1	1.4042	1.640E-8	8.600E-1	1.3038	2.150E-7
1.240E-1	1.4092	2.240E-1	1.950E-1	1.4007	1.590E-8	8.700E-1	1.3037	2.650E-7
1.272E-1	1.4026	1.950E-1	2.100E-1	1.3800	1.325E-8	8.800E-1	1.3035	3.350E-7
1.295E-1	1.3801	1.740E-1	2.500E-1	1.3509	8.623E-9	8.900E-1	1.3033	3.920E-7
1.305E-1	1.3630	1.720E-1	3.000E-1	1.3339	5.504E-9	9.000E-1	1.3032	4.200E-7
1.319E-1	1.3414	1.800E-1	3.500E-1	1.3249	3.765E-9	9.100E-1	1.3030	4.440E-7
1.333E-1	1.3238	1.940E-1	4.000E-1	1.3194	2.710E-9	9.200E-1	1.3028	4.740E-7
1.348E-1	1.3060	2.130E-1	4.100E-1	1.3185	2.510E-9	9.300E-1	1.3027	5.110E-7
1.362E-1	1.2905	2.430E-1	4.200E-1	1.3177	2.260E-9	9.400E-1	1.3025	5.530E-7
1.370E-1	1.2889	2.710E-1	4.300E-1	1.3170	2.080E-9	9.500E-1	1.3023	6.020E-7
1.378E-1	1.2893	2.890E-1	4.400E-1	1.3163	1.910E-9	9.600E-1	1.3022	7.550E-7
1.387E-1	1.3019	3.340E-1	4.500E-1	1.3157	1.540E-9	9.700E-1	1.3020	9.260E-7

$\lambda(\mu m)$	m_{re}	m_{im}	$\lambda(\mu m)$	m_{re}	m_{im}	$\lambda(\mu m)$	m_{re}	m_{im}
9.800E-1	1.3018	1.120E-6	1.504E+0	1.2915	5.899E-4	2.550E+0	1.2155	8.920E-4
9.900E-1	1.3017	1.330E-6	1.515E+0	1.2913	5.635E-4	2.565E+0	1.2118	8.700E-4
1.000E+0	1.3015	1.620E-6	1.527E+0	1.2911	5.480E-4	2.580E+0	1.2079	8.900E-4
1.010E+0	1.3013	2.000E-6	1.538E+0	1.2908	5.266E-4	2.590E+0	1.2051	9.300E-4
1.020E+0	1.3012	2.250E-6	1.563E+0	1.2903	4.394E-4	2.600E+0	1.2021	1.010E-3
1.030E+0	1.3010	2.330E-6	1.587E+0	1.2896	3.701E-4	2.620E+0	1.1957	1.350E-3
1.040E+0	1.3008	2.330E-6	1.613E+0	1.2889	3.372E-4	2.675E+0	1.1741	3.420E-3
1.050E+0	1.3006	2.170E-6	1.650E+0	1.2878	2.410E-4	2.725E+0	1.1473	7.920E-3
1.060E+0	1.3005	1.960E-6	1.680E+0	1.2869	1.890E-4	2.778E+0	1.1077	2.000E-2
1.070E+0	1.3003	1.810E-6	1.700E+0	1.2862	1.660E-4	2.817E+0	1.0674	3.800E-2
1.080E+0	1.3001	1.740E-6	1.730E+0	1.2852	1.450E-4	2.833E+0	1.0476	5.200E-2
1.090E+0	1.3000	1.730E-6	1.760E+0	1.2841	1.280E-4	2.849E+0	1.0265	6.800E-2
1.100E+0	1.2998	1.700E-6	1.800E+0	1.2826	1.030E-4	2.865E+0	1.0036	9.230E-2
1.110E+0	1.2996	1.760E-6	1.830E+0	1.2814	8.600E-5	2.882E+0	0.9820	1.270E-1
1.120E+0	1.2995	1.820E-6	1.840E+0	1.2809	8.220E-5	2.899E+0	0.9650	1.690E-1
1.130E+0	1.2993	2.040E-6	1.850E+0	1.2805	8.030E-5	2.915E+0	0.9596	2.210E-1
1.140E+0	1.2991	2.250E-6	1.855E+0	1.2802	8.500E-5	2.933E+0	0.9727	2.760E-1
1.150E+0	1.2989	2.290E-6	1.860E+0	1.2800	9.900E-5	2.950E+0	0.9917	3.120E-1
1.160E+0	1.2987	3.040E-6	1.870E+0	1.2795	1.500E-4	2.967E+0	1.0067	3.470E-1
1.170E+0	1.2985	3.840E-6	1.890E+0	1.2785	2.950E-4	2.985E+0	1.0219	3.880E-1
1.180E+0	1.2984	4.770E-6	1.905E+0	1.2777	4.687E-4	3.003E+0	1.0427	4.380E-1
1.190E+0	1.2982	5.760E-6	1.923E+0	1.2769	7.615E-4	3.021E+0	1.0760	4.930E-1
1.200E+0	1.2980	6.710E-6	1.942E+0	1.2761	1.010E-3	3.040E+0	1.1295	5.540E-1
1.210E+0	1.2978	8.660E-6	1.961E+0	1.2754	1.313E-3	3.058E+0	1.2127	6.120E-1
1.220E+0	1.2976	1.020E-5	1.980E+0	1.2747	1.539E-3	3.077E+0	1.3251	6.250E-1
1.230E+0	1.2974	1.130E-5	2.000E+0	1.2740	1.588E-3	3.096E+0	1.4260	5.930E-1
1.240E+0	1.2972	1.220E-5	2.020E+0	1.2733	1.540E-3	3.115E+0	1.4966	5.390E-1
1.250E+0	1.2970	1.290E-5	2.041E+0	1.2724	1.412E-3	3.135E+0	1.5510	4.910E-1
1.260E+0	1.2969	1.320E-5	2.062E+0	1.2714	1.244E-3	3.155E+0	1.5999	4.380E-1
1.270E+0	1.2967	1.350E-5	2.083E+0	1.2703	1.068E-3	3.175E+0	1.6363	3.720E-1
1.280E+0	1.2965	1.330E-5	2.105E+0	1.2690	8.414E-4	3.195E+0	1.6502	3.000E-1
1.290E+0	1.2963	1.320E-5	2.130E+0	1.2674	5.650E-4	3.215E+0	1.6428	2.380E-1
1.300E+0	1.2961	1.320E-5	2.150E+0	1.2659	4.320E-4	3.236E+0	1.6269	1.930E-1
1.310E+0	1.2958	1.310E-5	2.170E+0	1.2644	3.500E-4	3.257E+0	1.6128	1.580E-1
1.320E+0	1.2956	1.320E-5	2.190E+0	1.2628	2.870E-4	3.279E+0	1.5924	1.210E-1
1.330E+0	1.2954	1.320E-5	2.220E+0	1.2604	2.210E-4	3.300E+0	1.5733	1.030E-1
1.340E+0	1.2952	1.340E-5	2.240E+0	1.2586	2.030E-4	3.322E+0	1.5577	8.360E-2
1.350E+0	1.2950	1.390E-5	2.245E+0	1.2582	2.010E-4	3.345E+0	1.5413	6.680E-2
1.360E+0	1.2948	1.420E-5	2.250E+0	1.2577	2.030E-4	3.367E+0	1.5265	5.400E-2
1.370E+0	1.2945	1.480E-5	2.260E+0	1.2567	2.140E-4	3.390E+0	1.5114	4.220E-2
1.380E+0	1.2943	1.580E-5	2.270E+0	1.2558	2.320E-4	3.413E+0	1.4973	3.420E-2
1.390E+0	1.2941	1.740E-5	2.290E+0	1.2538	2.890E-4	3.436E+0	1.4845	2.740E-2
1.400E+0	1.2938	1.980E-5	2.310E+0	1.2518	3.810E-4	3.460E+0	1.4721	2.200E-2
1.410E+0	1.2936	2.500E-5	2.330E+0	1.2497	4.620E-4	3.484E+0	1.4612	1.860E-2
1.420E+0	1.2933	5.400E-5	2.350E+0	1.2475	5.480E-4	3.509E+0	1.4513	1.520E-2
1.430E+0	1.2930	1.040E-4	2.370E+0	1.2451	6.180E-4	3.534E+0	1.4421	1.260E-2
1.440E+0	1.2927	2.030E-4	2.390E+0	1.2427	6.800E-4	3.559E+0	1.4337	1.060E-2
1.449E+0	1.2925	2.708E-4	2.410E+0	1.2400	7.300E-4	3.624E+0	1.4155	8.020E-3
1.460E+0	1.2923	3.511E-4	2.430E+0	1.2373	7.820E-4	3.732E+0	1.3942	6.850E-3
1.471E+0	1.2921	4.299E-4	2.460E+0	1.2327	8.480E-4	3.775E+0	1.3873	6.600E-3
1.481E+0	1.2919	5.181E-4	2.500E+0	1.2258	9.250E-4	3.847E+0	1.3773	6.960E-3
1.493E+0	1.2917	5.855E-4	2.520E+0	1.2220	9.200E-4	3.969E+0	1.3645	9.160E-3

$\lambda(\mu m)$	m_{re}	m_{im}	$\lambda(\mu m)$	m_{re}	m_{im}	$\lambda(\mu m)$	m_{re}	m_{im}
4.099E+0	1.3541	1.110E-2	9.259E+0	1.2599	4.500E-2	3.333E+1	1.2642	1.060E-1
4.239E+0	1.3446	1.450E-2	9.524E+0	1.2451	4.600E-2	3.448E+1	1.2366	1.350E-1
4.348E+0	1.3388	2.000E-2	9.804E+0	1.2224	4.700E-2	3.564E+1	1.2166	1.761E-1
4.387E+0	1.3381	2.300E-2	1.000E+1	1.1991	5.100E-2	3.700E+1	1.2023	2.229E-1
4.444E+0	1.3385	2.600E-2	1.020E+1	1.1715	6.500E-2	3.824E+1	1.1964	2.746E-1
4.505E+0	1.3405	2.900E-2	1.031E+1	1.1553	7.500E-2	3.960E+1	1.1997	3.280E-1
4.547E+0	1.3429	2.930E-2	1.042E+1	1.1370	8.800E-2	4.114E+1	1.2086	3.906E-1
4.560E+0	1.3442	3.000E-2	1.053E+1	1.1181	1.080E-1	4.276E+1	1.2217	4.642E-1
4.580E+0	1.3463	2.850E-2	1.064E+1	1.1013	1.340E-1	4.358E+1	1.2417	5.247E-1
4.719E+0	1.3442	1.730E-2	1.075E+1	1.0908	1.680E-1	4.458E+1	1.2818	5.731E-1
4.904E+0	1.3345	1.290E-2	1.087E+1	1.0873	2.040E-1	4.550E+1	1.3278	6.362E-1
5.000E+0	1.3290	1.200E-2	1.100E+1	1.0925	2.480E-1	4.615E+1	1.3866	6.839E-1
5.100E+0	1.3233	1.250E-2	1.111E+1	1.1065	2.800E-1	4.671E+1	1.4649	7.091E-1
5.200E+0	1.3180	1.340E-2	1.136E+1	1.1478	3.410E-1	4.736E+1	1.5532	6.790E-1
5.263E+0	1.3143	1.400E-2	1.163E+1	1.2020	3.790E-1	4.800E+1	1.6038	6.250E-1
5.400E+0	1.3062	1.750E-2	1.190E+1	1.2582	4.090E-1	4.878E+1	1.6188	5.654E-1
5.556E+0	1.2972	2.400E-2	1.220E+1	1.3231	4.220E-1	5.003E+1	1.6296	5.433E-1
5.714E+0	1.2890	3.500E-2	1.250E+1	1.3857	4.220E-1	5.128E+1	1.6571	5.292E-1
5.747E+0	1.2873	3.800E-2	1.282E+1	1.4448	4.030E-1	5.275E+1	1.6981	5.070E-1
5.780E+0	1.2860	4.200E-2	1.299E+1	1.4717	3.890E-1	5.350E+1	1.7206	4.883E-1
5.814E+0	1.2851	4.600E-2	1.316E+1	1.4962	3.740E-1	5.424E+1	1.7486	4.707E-1
5.848E+0	1.2854	5.200E-2	1.333E+1	1.5165	3.540E-1	5.500E+1	1.7674	4.203E-1
5.882E+0	1.2881	5.700E-2	1.351E+1	1.5333	3.350E-1	5.574E+1	1.7648	3.771E-1
6.061E+0	1.3016	6.900E-2	1.370E+1	1.5490	3.150E-1	5.640E+1	1.7501	3.376E-1
6.135E+0	1.3090	7.000E-2	1.389E+1	1.5628	2.940E-1	5.700E+1	1.7233	3.056E-1
6.250E+0	1.3172	6.700E-2	1.408E+1	1.5732	2.710E-1	5.746E+1	1.6849	2.835E-1
6.289E+0	1.3189	6.500E-2	1.429E+1	1.5803	2.460E-1	5.840E+1	1.6240	3.170E-1
6.329E+0	1.3204	6.400E-2	1.471E+1	1.5792	1.980E-1	5.929E+1	1.5960	3.517E-1
6.369E+0	1.3220	6.200E-2	1.515E+1	1.5667	1.640E-1	6.000E+1	1.5851	3.902E-1
6.410E+0	1.3224	5.900E-2	1.538E+1	1.5587	1.520E-1	6.100E+1	1.5992	4.509E-1
6.452E+0	1.3215	5.700E-2	1.563E+1	1.5508	1.420E-1	6.125E+1	1.6140	4.671E-1
6.494E+0	1.3204	5.600E-2	1.613E+1	1.5381	1.280E-1	6.250E+1	1.6662	4.779E-1
6.579E+0	1.3181	5.500E-2	1.639E+1	1.5330	1.250E-1	6.378E+1	1.7066	4.890E-1
6.667E+0	1.3171	5.700E-2	1.667E+1	1.5322	1.230E-1	6.467E+1	1.7371	4.899E-1
6.757E+0	1.3181	5.800E-2	1.695E+1	1.5334	1.160E-1	6.558E+1	1.7686	4.873E-1
6.897E+0	1.3195	5.700E-2	1.724E+1	1.5329	1.070E-1	6.655E+1	1.8034	4.766E-1
7.042E+0	1.3193	5.500E-2	1.818E+1	1.5170	7.900E-2	6.760E+1	1.8330	4.508E-1
7.143E+0	1.3190	5.500E-2	1.887E+1	1.5010	7.200E-2	6.900E+1	1.8568	4.193E-1
7.246E+0	1.3191	5.400E-2	1.923E+1	1.4968	7.600E-2	7.053E+1	1.8741	3.880E-1
7.353E+0	1.3180	5.200E-2	1.961E+1	1.4993	7.500E-2	7.300E+1	1.8911	3.433E-1
7.463E+0	1.3163	5.200E-2	2.000E+1	1.5015	6.700E-2	7.500E+1	1.8992	3.118E-1
7.576E+0	1.3154	5.200E-2	2.041E+1	1.4986	5.500E-2	7.629E+1	1.9043	2.935E-1
7.692E+0	1.3154	5.200E-2	2.083E+1	1.4905	4.500E-2	8.000E+1	1.9033	2.350E-1
7.812E+0	1.3155	5.000E-2	2.222E+1	1.4607	2.900E-2	8.297E+1	1.8874	1.981E-1
7.937E+0	1.3145	4.700E-2	2.260E+1	1.4518	2.750E-2	8.500E+1	1.8750	1.865E-1
8.065E+0	1.3119	4.300E-2	2.305E+1	1.4422	2.700E-2	8.680E+1	1.8670	1.771E-1
8.197E+0	1.3068	3.900E-2	2.360E+1	1.4316	2.730E-2	9.080E+1	1.8536	1.620E-1
8.333E+0	1.2993	3.700E-2	2.460E+1	1.4138	2.890E-2	9.517E+1	1.8425	1.490E-1
8.475E+0	1.2925	3.900E-2	2.500E+1	1.4068	3.000E-2	1.000E+2	1.8323	1.390E-1
8.696E+0	1.2839	4.000E-2	2.600E+1	1.3895	3.400E-2	1.200E+2	1.8191	1.200E-1
8.929E+0	1.2740	4.200E-2	2.857E+1	1.3489	5.300E-2	1.500E+2	1.8227	9.620E-2
9.091E+0	1.2672	4.400E-2	3.100E+1	1.3104	7.550E-2	1.670E+2	1.8296	8.300E-2

A. Ultraviolet, 185–400 nm

Only liquid-water data are now available, and they cannot be used for ice because ice absorption is very likely to be considerably weaker than that of water in this spectral region. The absorption coefficient here is so small that it can be taken as zero in many applications. However, for some purposes, such as radiative transfer calculations for optically thick media,[5] the correct nonzero values are required.

B. Near-Infrared, 1.4–2.8 μm

The measurements now available (Fig. 4) are in conflict and are of questionable accuracy because of inappropriate or inadequately known sample thickness and the possibility of significant light scattering in the samples used.

C. Middle-Infrared, 3.5–4.3 μm

The imaginary index is too small here to be obtained accurately by the reflection measurements of Schaaf and Williams[10]; their values, while accurate elsewhere, are uncertain to ±50% in this narrow wavelength interval. Transmission measurements would be desirable.

D. Far-Infrared, 33–600 μm

Measurements were made at T = 100 K, and a considerable temperature dependence was shown between 100 and 168 K. Measurements at higher temperatures are not available. This spectral region is of use for some geophysical applications (cooling to space by cirrus and stratospheric clouds), and these measurements are also needed in order to do the dispersion analysis to obtain m_{re} and m_{im} in the middle-infrared, $\lambda < 33$ μm.

E. Microwave and Radiowave, 1.25 mm–2 m

(1) There are no reliable measurements betweeen 1.25 and 12.5 mm.

(2) Different sets of apparently reliable measurements between 12.5 and 110 mm are in mutual conflict. The favored measurements are those of Cumming,[44] but these apparently disagree with the theoretical extrapolation of Mishima *et al.*[8]

(3) For 110 mm–2 m it would be desirable to obtain additional measurements to confirm or dispute our choice of Westphal's unpublished measurements,[17] since they conflict with other available measurements.

I thank Dennis Klug and Edward Whalley for prepublication results of their far-infrared measurements, Koichi Kobayashi for expanded graphs of his ultraviolet measurements, and Nathan Ockman for being able to locate an absorption spectrum plot that was not included in his thesis. John Bertie, Gyan Johari, and Frederick Reding provided useful advice. Craig Bohren carefully reviewed both the first and final drafts of this paper. An anonymous reviewer also made helpful suggestions. This work was supported by NSF grants ATM-80-24641, ATM-82-06318, and ATM-82-15337. The computations were done at the National Center for Atmospheric Research. This is Contribution No. 693 from the Department of Atmospheric Sciences, University of Washington.

References

1. W. M. Irvine and J. B. Pollack, Icarus **8,** 324 (1968).
2. S. Evans, J. Glaciol. **5,** 773 (1965).
3. P. S. Ray, Appl. Opt. **11,** 1836 (1972).
4. P. V. Hobbs, *Ice Physics* (Clarendon, Oxford, 1974).
5. W. J. Wiscombe and S. G. Warren, J. Atmos. Sci. **37,** 2712 (1980).
6. E. Whalley, J. Phys. Chem. **87,** 4174 (1983).
7. M. Seki, K. Kobayashi, and J. Nakahara, J. Phys. Soc. Jpn. **50,** 2643 (1981).
8. O. Mishima, D. D. Klug, and E. Whalley, J. Chem. Phys. **78,** 6399 (1983).
9. G. P. Johari, Contemp. Phys. **22,** 613 (1981).
10. J. W. Schaaf and D. Williams, J. Opt. Soc. Am. **63,** 726 (1973).
11. J. E. Bertie, H. J. Labbé, and E. Whalley, J. Chem. Phys. **50,** 4501 (1969).
12. T. C. Grenfell and D. K. Perovich, J. Geophys. Res. **86,** 7447 (1981).
13. J. D. Neufeld and G. Andermann, J. Opt. Soc. Am. **62,** 1156 (1972).
14. G. M. Hale and M. R. Querry, Appl. Opt. **12,** 555 (1973).
15. H. E. Merwin, "Refractivity of Birefringent Crystals," in *International Critical Tables* (McGraw-Hill, New York, 1930), Vol. 7, pp. 16–33.
16. S. R. Gough, Can. J. Chem. **50,** 3046 (1972).
17. G. R. Jiracek, "Radio Sounding of Antarctic Ice," in Research Report 67-1, (Geophysical and Polar Research Center, U. Wisconsin, 1967).
18. J. B. Hasted, *Aqueous Dielectrics* (Chapman & Hall, London, 1973).
19. J. Daniels, Opt. Commun. **3,** 240 (1971).
20. R. Onaka and T. Takahashi, J. Phys. Soc. Jpn. **24,** 548 (1968).
21. A. Otto and M. J. Lynch, Aust. J. Phys. **23,** 609 (1970).
22. K. Dressler and O. Schnepp, J. Chem. Phys. **33,** 270 (1960).
23. E. V. Browell and R. C. Anderson, J. Opt. Soc. Am. **65,** 919 (1975).

References are continued on page 1225.

Table II. Real (m_{re}) and imaginary (m_{im}) parts of the complex index of refraction of ice Ih, from 167-μm to 8.6-m wavelength (λ), for four temperatures (T). These values are graphed in Figs. 11 (c) and (f). For intermediate wavelengths not given in the table, one should interpolate m_{re} linearly in logλ, logm_{im} linearly in logλ, m_{re} linearly in T, and logm_{im} linearly in T. Table II is on the next page.

	T = -1°C		T = -5°C		T = -20°C		T = -60°C	
λ(μm)	m_{re}	m_{im}	m_{re}	m_{im}	m_{re}	m_{im}	m_{re}	m_{im}
1.670E+2	1.8296	8.300E-2	1.8296	8.300E-2	1.8296	8.300E-2	1.8296	8.300E-2
1.778E+2	1.8326	6.900E-2	1.8326	6.900E-2	1.8326	6.900E-2	1.8326	6.900E-2
1.884E+2	1.8315	5.700E-2	1.8315	5.700E-2	1.8315	5.700E-2	1.8315	5.700E-2
1.995E+2	1.8275	4.560E-2	1.8275	4.560E-2	1.8275	4.560E-2	1.8275	4.450E-2
2.113E+2	1.8222	3.790E-2	1.8222	3.790E-2	1.8222	3.790E-2	1.8222	3.550E-2
2.239E+2	1.8172	3.140E-2	1.8172	3.140E-2	1.8172	3.140E-2	1.8172	2.910E-2
2.371E+2	1.8120	2.620E-2	1.8120	2.620E-2	1.8120	2.620E-2	1.8120	2.440E-2
2.512E+2	1.8070	2.240E-2	1.8070	2.240E-2	1.8070	2.190E-2	1.8070	1.970E-2
2.661E+2	1.8025	1.960E-2	1.8025	1.960E-2	1.8025	1.880E-2	1.8025	1.670E-2
2.818E+2	1.7983	1.760E-2	1.7983	1.760E-2	1.7983	1.660E-2	1.7983	1.400E-2
2.985E+2	1.7948	1.665E-2	1.7948	1.665E-2	1.7948	1.540E-2	1.7948	1.235E-2
3.162E+2	1.7921	1.620E-2	1.7921	1.600E-2	1.7921	1.470E-2	1.7921	1.080E-2
3.548E+2	1.7884	1.550E-2	1.7884	1.500E-2	1.7884	1.350E-2	1.7884	8.900E-3
3.981E+2	1.7860	1.470E-2	1.7860	1.400E-2	1.7860	1.250E-2	1.7860	7.340E-3
4.467E+2	1.7843	1.390E-2	1.7843	1.310E-2	1.7843	1.150E-2	1.7843	6.400E-3
5.012E+2	1.7832	1.320E-2	1.7832	1.230E-2	1.7832	1.060E-2	1.7832	5.600E-3
5.623E+2	1.7825	1.250E-2	1.7825	1.150E-2	1.7825	9.770E-3	1.7825	5.000E-3
6.310E+2	1.7820	1.180E-2	1.7820	1.080E-2	1.7820	9.010E-3	1.7820	4.520E-3
7.943E+2	1.7817	1.060E-2	1.7817	9.460E-3	1.7816	7.660E-3	1.7815	3.680E-3
1.000E+3	1.7816	9.540E-3	1.7816	8.290E-3	1.7814	6.520E-3	1.7807	2.990E-3
1.259E+3	1.7819	8.560E-3	1.7819	7.270E-3	1.7816	5.540E-3	1.7801	2.490E-3
2.500E+3	1.7830	6.210E-3	1.7830	4.910E-3	1.7822	3.420E-3	1.7789	1.550E-3
5.000E+3	1.7843	4.490E-3	1.7843	3.300E-3	1.7831	2.100E-3	1.7779	9.610E-4
1.000E+4	1.7852	3.240E-3	1.7852	2.220E-3	1.7838	1.290E-3	1.7773	5.950E-4
2.000E+4	1.7862	2.340E-3	1.7861	1.490E-3	1.7839	7.930E-4	1.7772	3.690E-4
3.200E+4	1.7866	1.880E-3	1.7863	1.140E-3	1.7840	5.700E-4	1.7772	2.670E-4
3.500E+4	1.7868	1.740E-3	1.7864	1.060E-3	1.7840	5.350E-4	1.7772	2.510E-4
4.000E+4	1.7869	1.500E-3	1.7865	9.480E-4	1.7840	4.820E-4	1.7772	2.290E-4
4.500E+4	1.7870	1.320E-3	1.7865	8.500E-4	1.7840	4.380E-4	1.7772	2.110E-4
5.000E+4	1.7870	1.160E-3	1.7865	7.660E-4	1.7840	4.080E-4	1.7772	1.960E-4
6.000E+4	1.7871	8.800E-4	1.7865	6.300E-4	1.7839	3.500E-4	1.7772	1.730E-4
7.000E+4	1.7871	6.950E-4	1.7865	5.200E-4	1.7838	3.200E-4	1.7772	1.550E-4
9.000E+4	1.7872	4.640E-4	1.7865	3.840E-4	1.7837	2.550E-4	1.7772	1.310E-4
1.110E+5	1.7872	3.400E-4	1.7865	2.960E-4	1.7837	2.120E-4	1.7772	1.130E-4
1.200E+5	1.7872	3.110E-4	1.7865	2.700E-4	1.7837	2.000E-4	1.7772	1.060E-4
1.300E+5	1.7872	2.940E-4	1.7865	2.520E-4	1.7837	1.860E-4	1.7772	9.900E-5
1.400E+5	1.7872	2.790E-4	1.7865	2.440E-4	1.7837	1.750E-4	1.7772	9.300E-5
1.500E+5	1.7872	2.700E-4	1.7865	2.360E-4	1.7837	1.660E-4	1.7772	8.730E-5
1.600E+5	1.7872	2.640E-4	1.7865	2.300E-4	1.7837	1.560E-4	1.7772	8.300E-5
1.700E+5	1.7872	2.580E-4	1.7865	2.280E-4	1.7837	1.490E-4	1.7772	7.870E-5
1.800E+5	1.7872	2.520E-4	1.7865	2.250E-4	1.7837	1.440E-4	1.7772	7.500E-5
2.000E+5	1.7872	2.490E-4	1.7865	2.200E-4	1.7837	1.350E-4	1.7772	6.830E-5
2.500E+5	1.7872	2.540E-4	1.7865	2.160E-4	1.7837	1.210E-4	1.7772	5.600E-5
2.900E+5	1.7872	2.640E-4	1.7865	2.170E-4	1.7837	1.160E-4	1.7772	4.960E-5
3.200E+5	1.7872	2.740E-4	1.7865	2.200E-4	1.7837	1.160E-4	1.7772	4.550E-5
3.500E+5	1.7872	2.890E-4	1.7865	2.250E-4	1.7837	1.170E-4	1.7772	4.210E-5
3.800E+5	1.7872	3.050E-4	1.7865	2.320E-4	1.7837	1.200E-4	1.7772	3.910E-5
4.000E+5	1.7872	3.150E-4	1.7865	2.390E-4	1.7837	1.230E-4	1.7772	3.760E-5
4.500E+5	1.7872	3.460E-4	1.7865	2.600E-4	1.7837	1.320E-4	1.7772	3.400E-5
5.000E+5	1.7872	3.820E-4	1.7865	2.860E-4	1.7837	1.440E-4	1.7772	3.100E-5
6.000E+5	1.7872	4.620E-4	1.7865	3.560E-4	1.7837	1.680E-4	1.7772	2.640E-5
6.400E+5	1.7872	5.000E-4	1.7865	3.830E-4	1.7837	1.800E-4	1.7772	2.510E-5
6.800E+5	1.7872	5.500E-4	1.7865	4.150E-4	1.7837	1.900E-4	1.7772	2.430E-5
7.200E+5	1.7872	5.950E-4	1.7865	4.450E-4	1.7837	2.090E-4	1.7772	2.390E-5
7.600E+5	1.7872	6.470E-4	1.7865	4.760E-4	1.7837	2.160E-4	1.7772	2.370E-5
8.000E+5	1.7872	6.920E-4	1.7865	5.080E-4	1.7837	2.290E-4	1.7772	2.380E-5
8.400E+5	1.7872	7.420E-4	1.7865	5.400E-4	1.7837	2.400E-4	1.7772	2.400E-5
9.000E+5	1.7872	8.200E-4	1.7865	5.860E-4	1.7837	2.600E-4	1.7772	2.460E-5
1.000E+6	1.7872	9.700E-4	1.7865	6.780E-4	1.7837	2.920E-4	1.7772	2.660E-5
2.000E+6	1.7872	1.950E-3	1.7865	1.280E-3	1.7837	6.100E-4	1.7772	4.450E-5
5.000E+6	1.7872	5.780E-3	1.7865	3.550E-3	1.7840	1.020E-3	1.7772	8.700E-5
8.600E+6	1.7880	9.700E-3	1.7872	5.600E-3	1.7845	1.810E-3	1.7780	1.320E-4

24. T. Shibaguchi, H. Onuki, and R. Onaka, J. Phys. Soc. Jpn. **42,** 152 (1977).
25. A. P. Minton, J. Phys. Chem. **75,** 1162 (1971).
26. L. R. Painter, R. D. Birkhoff, and E. T. Arakawa, J. Chem. Phys. **51,** 243 (1969).
27. F. Sauberer, Wetter Leben **2,** 193 (1950).
28. T. C. Grenfell, J. Glaciol. **27,** 476 (1981).
29. W. Luck, Ber. Bunsenges. Phys. Chem. **67,** 186 (1963).
30. F. P. Reding, "The Vibrational Spectrum and Structure of Several Molecular Crystals at Low Temperature," Ph.D. Thesis, Brown U., Providence, R.I. (1951).
31. D. F. Hornig, H. F. White, and F. P. Reding, Spectrochim. Acta **12,** 338 (1958).
32. N. Ockman, "The Infrared-Spectra and Raman-Spectra of Single Crystals of Ordinary Ice," Ph.D. Thesis, U. Michigan, Ann Arbor (1957).
33. R. N. Clark, J. Geophys. Res. **86,** 3087 (1981).
34. U. Fink and H. P. Larson, Icarus **24,** 411 (1975).
35. N. Ockman, Adv. Phys. **7,** 199 (1958).
36. M. S. Bergren, D. Schuh, M. G. Sceats, and S. A. Rice, J. Chem. Phys. **69,** 3477 (1978).
37. S. Tsujimoto, A. Konishi, and T. Kunitomo, Cryogenics **22,** 603 (1982).
38. J. E. Bertie and E. Whalley, J. Chem. Phys. **46,** 1271 (1967).
39. A. Léger, S. Gauthier, D. Défourneau, and D. Rouan, Astron. Astrophys. **117,** 164 (1983).
40. E. Whalley and H. J. Labbé, J. Chem. Phys. **51,** 3120 (1969).
41. R. Zimmermann and G. C. Pimentel, *Advances in Molecular Spectroscopy*, (Macmillan, New York, 1962), Vol. 2, pp. 726–737.
42. J. Lamb, Discuss. Faraday Soc. **42A,** 238 (1946).
43. J. Lamb and A. Turney, Proc. Phys. Soc. London Sect. B **62,** 272 (1949).
44. W. A. Cumming, J. Appl. Phys. **23,** 768 (1952).
45. J. W. Perry and A. W. Straiton, J. Appl. Phys. **44,** 5180 (1973).
46. S. R. Gough, J. Appl. Phys. **43,** 4251 (1972).
47. J. W. Perry and A. W. Straiton, J. Appl. Phys. **43,** 731 (1972).
48. M. R. Vant, R. B. Gray, R. O. Ramseier, and V. Makios, J. Appl. Phys. **45,** 4712 (1974).
49. R. H. Ragle, R. G. Blair, and L. E. Persson, J. Glaciol. **5,** 39 (1964).
50. R. S. Vickers, "Microwave Properties of Ice from the Great Lakes," NASA Contract. Rep. 135222 (1977).
51. A. von Hippel, *Tables of Dielectric Materials* (MIT Press, Cambridge, 1945).
52. T. Yoshino, Antarct. Rec. **11,** 228 (1961).
53. G. P. Johari and P. A. Charette, J. Glaciol. **14,** 293 (1975).
54. G. P. Johari, J. Chem. Phys. **64,** 3998 (1976).
55. P. M. Champion and A. J. Sievers, J. Chem. Phys. **72,** 1569 (1980).
56. H. D. Downing and D. Williams, J. Geophys. Res. **80,** 1656 (1975).
57. R. K. Ahrenkiel, J. Opt. Soc. Am. **61,** 1651 (1971).
58. R. Z. Bachrach and F. C. Brown, Phys. Rev. B **1,** 818 (1970).
59. E. Gilberg, M. J. Hanus, and B. Foltz, J. Chem. Phys. **76,** 5093 (1982).